JEM Journal of Experimental Medicine

ARTICLE

Disruption of FBXL5-mediated cellular iron homeostasis promotes liver carcinogenesis

Yoshiharu Muto[1*], Toshiro Moroishi[1*], Kazuya Ichihara[1], Masaaki Nishiyama[1], Hideyuki Shimizu[1], Hidetoshi Eguchi[2], Kyoji Moriya[3], Kazuhiko Koike[4], Koshi Mimori[5], Masaki Mori[2], Yuta Katayama[1], and Keiichi I. Nakayama[1]

Hepatic iron overload is a risk factor for progression of hepatocellular carcinoma (HCC), although the molecular mechanisms underlying this association have remained unclear. We now show that the iron-sensing ubiquitin ligase FBXL5 is a previously unrecognized oncosuppressor in liver carcinogenesis in mice. Hepatocellular iron overload elicited by FBXL5 ablation gave rise to oxidative stress, tissue damage, inflammation, and compensatory proliferation of hepatocytes and to consequent promotion of liver carcinogenesis induced by exposure to a chemical carcinogen. The tumor-promoting outcome of FBXL5 deficiency in the liver was also found to be effective in a model of virus-induced HCC. FBXL5-deficient mice thus constitute the first genetically engineered mouse model of liver carcinogenesis promoted by iron overload. In addition, dysregulation of FBXL5-mediated cellular iron homeostasis was found to be associated with poor prognosis in human HCC, suggesting that FBXL5 plays a key role in defense against hepatocarcinogenesis.

Introduction

Hepatocellular carcinoma (HCC) is one of the most lethal and prevalent cancers worldwide. The molecular, cellular, and environmental underpinnings of HCC development and progression remain unclear, however, and few therapeutic options are available. Prominent factors associated with HCC include chronic hepatitis B or C virus infection, long-term alcohol intake, consumption of aflatoxin B1–contaminated food, and metabolic disorders such as nonalcoholic fatty liver disease and hereditary hemochromatosis (El-Serag, 2011). These factors are also associated with liver damage due to inflammation and oxidative stress (Farazi and DePinho, 2006). Oxidative stress in the liver promotes cell death and subsequent compensatory proliferation of hepatocytes (Kamata et al., 2005), with these effects being associated with modification of intracellular signaling pathways and the accumulation of genetic alterations that eventually lead to malignant progression (Maeda et al., 2005; Luedde et al., 2014; Marquardt et al., 2015). Homeostasis of cellular iron, a major elicitor of oxidative stress, is therefore likely integral to defense against hepatocarcinogenesis.

Iron is an essential factor for many metabolic processes in cells and organisms and also functions as cofactors such as heme and iron-sulfur clusters. On the other hand, iron catalyzes the Fenton reaction that results in generation of the hydroxyl radical, one of the most detrimental ROS in vivo that damages many biological macromolecules. It is therefore important that cellular iron levels undergo strict regulation (Hentze et al., 2010). Cellular iron level was shown to be regulated predominantly by F-box and leucine-rich repeat protein 5 (FBXL5) and iron regulatory protein 2 (IRP2) in vivo (Moroishi et al., 2011). IRP2 is an RNA-binding protein that regulates the translation and stability of mRNAs encoding proteins that contribute to cellular iron homeostasis. Based on these actions, IRP2 regulates the size of the available iron pool in a manner dependent on cellular iron concentration. Under iron-replete conditions, the SCF^{FBXL5} E3 ubiquitin ligase complex mediates the ubiquitylation and degradation of IRP2, with FBXL5 serving as the substrate recognition component for IRP2. Binding of iron to the hemerythrin domain of FBXL5 stabilizes this protein, whereas FBXL5 is unstable under iron-deficient conditions. This iron-sensing ability

[1]Department of Molecular and Cellular Biology, Medical Institute of Bioregulation, Kyushu University, Fukuoka, Japan; [2]Department of Gastroenterological Surgery, Graduate School of Medicine, Osaka University, Suita, Japan; [3]Department of Infection Control and Prevention, The University of Tokyo Hospital, Tokyo, Japan; [4]Department of Gastroenterology, Graduate School of Medicine, The University of Tokyo, Tokyo, Japan; [5]Department of Surgery, Kyushu University, Beppu Hospital, Beppu, Japan.

*Y. Muto and T. Moroishi contributed equally to this paper; Correspondence to Keiichi I. Nakayama: nakayak1@bioreg.kyushu-u.ac.jp; Masaaki Nishiyama: nishiyam@staff.kanazawa-u.ac.jp; Y. Muto's present address is Division of Nephrology, Department of Medicine, Washington University School of Medicine, St. Louis, MO; T. Moroishi's present address is Department of Molecular Enzymology and Center for Metabolic Regulation of Healthy Aging, Faculty of Life Sciences, Kumamoto University, Kumamoto, Japan; M. Nishiyama's present address is Department of Histology and Cell Biology, Graduate School of Medical Sciences, Kanazawa University, Kanazawa, Japan.

allows FBXL5 to control the abundance of IRP2 in an iron-dependent manner (Salahudeen et al., 2009; Vashisht et al., 2009). Mice deficient in FBXL5 manifest the failure of cells to sense increased cellular iron availability, resulting in constitutive accumulation of IRP2 and aberrant expression of its target genes. FBXL5-null mice show early embryonic mortality as a result of overwhelming oxidative stress, suggesting the essential role of FBXL5 in cellular iron homeostasis during early embryogenesis (Moroishi et al., 2011; Ruiz et al., 2013).

A substantial proportion of iron in the adult body is present in the hematopoietic system and liver. Conditional deletion of *Fbxl5* in the hematopoietic system of mice results in iron overload in hematopoietic stem cells, with the consequent increase in oxidative stress impairing the ability of the cells to repopulate bone marrow (Muto et al., 2017). *FBXL5* expression was also shown to be down-regulated in hematopoietic stem cells of some patients with myelodysplastic syndrome, suggesting that disruption of cellular iron homeostasis might contribute to this disease (Nilsson et al., 2007; Muto et al., 2017). In addition, conditional FBXL5 deficiency in mouse liver was found to result in iron accumulation and mitochondrial dysfunction in hepatocytes, leading to the development of steatohepatitis (Moroishi et al., 2011).

Iron homeostasis in the liver has been implicated in the pathogenesis of liver cancer. Individuals with hereditary hemochromatosis manifest iron overload in the liver and other organs and have a 200-fold greater risk of HCC development compared with the general population (Niederau et al., 1996; Bacon et al., 2011). Down-regulation of hepcidin expression is a characteristic finding in the liver of hemochromatosis patients and has been shown to be the cause of hepatic iron overload and subsequent hepatocarcinogenesis in such patients (Bacon et al., 2011). Hepatic iron excess is also a risk factor for HCC development in patients with nonalcoholic fatty liver disease (Sorrentino et al., 2009; Valenti et al., 2010) or those infected with hepatitis C virus (HCV; Chapoutot et al., 2000), with iron depletion therapy by phlebotomy and low-iron diet therapy having been shown to lower the risk for HCC development in individuals with chronic HCV infection (Kato et al., 2007). In addition, hepatic iron accumulation or elevated serum iron levels have also been associated with chronic hepatitis B virus (HBV) infection (Felton et al., 1979; Senba et al., 1985) and to be correlated with the severity of HBV-related hepatitis (Martinelli et al., 2004; Mao et al., 2015). Furthermore, hepatic accumulation of iron was found to be predictive of HCC development (Nahon et al., 2008) or death (Ganne-Carrié et al., 2000) in patients with alcoholic cirrhosis. A clinical association between aflatoxin-induced HCC and iron overload has not been described to date, although exposure to aflatoxin B1 and dietary iron overload were shown to have a synergistic effect on the generation of oxidative stress or DNA damage in rat liver (Asare et al., 2007).

The abundance of hepcidin or FBXL5 mRNAs was found to be reduced in the liver of patients with chronic HCV infection (Fujita et al., 2007; Girelli et al., 2009; Nanba et al., 2016), further suggesting that altered iron homeostasis may be permissive for HCC in such patients. Moreover, hepcidin expression is down-regulated in the FBXL5-deficient mouse liver as a result of altered bone morphogenetic protein signaling (Moroishi et al., 2011), suggesting that the reduced amount of hepcidin mRNA in the liver of patients with chronic HCV infection might also result from dysregulation of FBXL5. In contrast, the abundance of hepcidin is increased in the liver of individuals with nonalcoholic steatohepatitis (Britton et al., 2016) or chronic HBV infection (Tseng et al., 2009), suggesting that down-regulation of hepcidin expression is not a universal mechanism for hepatic iron overload in chronic liver disease and that additional mechanisms remain to be elucidated.

Despite these various lines of evidence implicating iron dysregulation as a risk factor for liver cancer, the lack of a genetically engineered mouse model of hepatocarcinogenesis induced by hepatic iron overload has hampered research into pathogenic mechanisms. Here we provide evidence that altered FBXL5-mediated cellular iron homeostasis is associated with liver carcinogenesis, and that FBXL5-deficient mice constitute a genetically engineered mouse model of carcinogenesis promoted by dysregulation of iron homeostasis. We hypothesized that dysregulation of FBXL5 might promote the development of HCC on the basis of the previous epidemiologic and clinical findings. To validate such a promoting effect on tumorigenesis, we adopted the diethylnitrosamine (DEN)-induced HCC model, given that a single DEN injection acts as an initiator of hepatocarcinogenesis (Sarma et al., 1986). Hepatocellular iron overload evoked by FBXL5 ablation in mice gave rise to oxidative stress, tissue damage, inflammation, and compensatory proliferation of hepatocytes as well as to consequent promotion of liver carcinogenesis induced by DEN exposure. This tumor-promoting effect of FBXL5 deficiency was confirmed in a model of carcinogenesis induced by expression of HCV core antigen. Furthermore, we found that a low level of *FBXL5* expression in HCC patients is associated with poor prognosis, suggesting that the FBXL5–IRP2 axis is a potential therapeutic target for HCC associated with cellular iron dysregulation.

Results

FBXL5 is essential for defense against HCC

To explore the role of cellular iron homeostasis governed by FBXL5 in hepatocarcinogenesis, we generated mice in which *Fbxl5* is specifically deleted in the liver by crossing *Fbxl5*$^{F/F}$ mice (which harbor floxed alleles of *Fbxl5*) with *Alb*-Cre transgenic mice (which express Cre recombinase under the control of the albumin gene promoter). The resulting *Alb*-Cre/*Fbxl5*$^{F/F}$ mice do not develop liver tumors spontaneously until ∼750 d of age (data not shown), but they accumulate iron in the liver and develop steatohepatitis (Moroishi et al., 2011). We therefore investigated whether FBXL5 deficiency promotes liver carcinogenesis in association with exposure to a chemical carcinogen. A single administration of DEN to weaning male mice induces acute liver injury as well as the formation of multiple liver tumors within 10 mo (Sarma et al., 1986). Male *Alb*-Cre/*Fbxl5*$^{F/F}$ and *Fbxl5*$^{F/F}$ littermate control mice were thus injected i.p. with DEN at 15 d of age, and the resulting hepatic tumor nodules were examined at 36 wk of age (Fig. 1 A). *Alb*-Cre/*Fbxl5*$^{F/F}$ mice manifested a

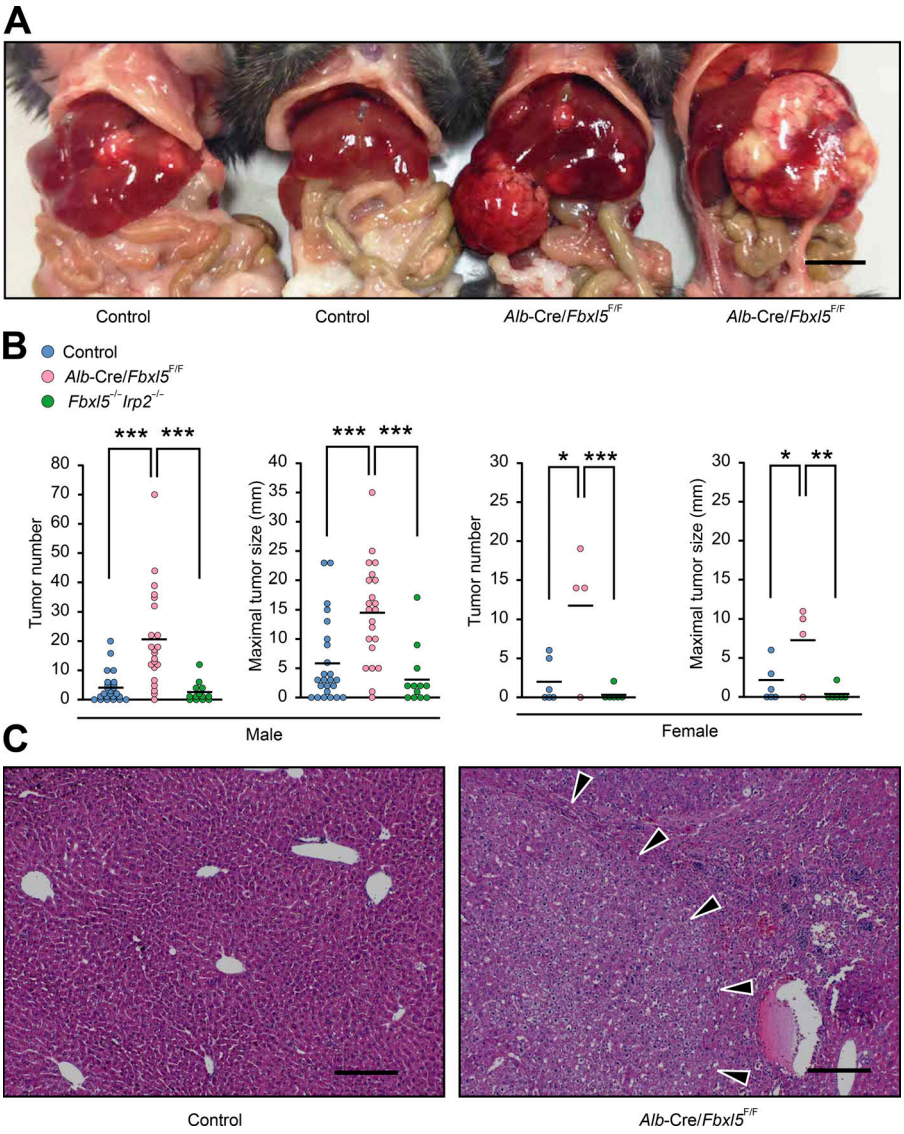

Figure 1. **FBXL5 deficiency promotes liver carcinogenesis. (A)** Gross appearance of the liver of DEN-injected *Fbxl5*$^{F/F}$ (control) and *Alb*-Cre/*Fbxl5*$^{F/F}$ male mouse littermates at 36 wk of age. Bar, 10 mm. **(B)** Tumor multiplicity and maximal tumor diameter for the liver of DEN-injected *Fbxl5*$^{F/F}$ (male, *n* = 24; female, *n* = 6), *Alb*-Cre/*Fbxl5*$^{F/F}$ (male, *n* = 22; female, *n* = 4), and *Fbxl5*$^{-/-}$*Irp2*$^{-/-}$ (male, *n* = 13; female, *n* = 6) mice at 36 wk of age. Horizontal bars are means. *, P < 0.05; **, P < 0.01; ***, P < 0.005 (one-way ANOVA followed by Tukey's test). **(C)** Hematoxylin-eosin staining of liver sections from DEN-injected *Fbxl5*$^{F/F}$ and *Alb*-Cre/*Fbxl5*$^{F/F}$ male mouse littermates at 36 wk of age. Arrowheads indicate a liver tumor. Bars, 200 µm.

higher tumor incidence and increased tumor size compared with *Fbxl5*$^{F/F}$ mice (Fig. 1 B). We also confirmed that FBXL5 deficiency promoted tumorigenesis in DEN-injected mice at 32 wk of age (Fig. S1). Histopathologic analysis of hepatic tissue sections also confirmed the increased number and size of tumorous lesions in the liver of *Alb*-Cre/*Fbxl5*$^{F/F}$ mice (Fig. 1 C). Of note, hepatic FBXL5 deficiency also promoted liver tumor development in female mice (Fig. 1 B), although females are less susceptible to DEN-induced liver carcinogenesis than are males (Naugler et al., 2007). Together, these data thus suggested that hepatic iron homeostasis governed by FBXL5 plays a prominent role in prevention of hepatocarcinogenesis.

To exclude the possibility that DNA damage potentially induced by Cre recombinase promotes liver carcinogenesis induced by exposure to DEN, we injected male *Alb*-Cre/*Fbxl5*$^{F/+}$ mice with DEN at 15 d of age and examined the incidence of hepatic tumor formation at 36 wk of age. *Alb*-Cre/*Fbxl5*$^{F/+}$ mice developed tumors with a number and size similar to those for *Fbxl5*$^{F/F}$ mice (Fig. S2 A). The survival rate of the DEN-injected *Alb*-Cre/*Fbxl5*$^{F/+}$ mice was also similar to that of control *Fbxl5*$^{F/F}$ mice (Fig. S2 B). We therefore concluded that Cre recombinase alone does not influence hepatic tumorigenesis in our experimental system.

Given that impaired degradation of IRP2 is primarily responsible for the embryonic mortality of *Fbxl5*$^{-/-}$ mice (Moroishi et al., 2011), we next investigated whether the promotion of carcinogenesis in the liver of *Alb*-Cre/*Fbxl5*$^{F/F}$ mice might also be attributable to IRP2 accumulation. Examination of DEN-induced carcinogenesis in the liver of male *Fbxl5*$^{-/-}$*Irp2*$^{-/-}$ mice revealed that the number and size of tumors at 36 wk of age were similar to those for *Fbxl5*$^{F/F}$ control mice (Fig. 1 B). Similar effects of IRP2 ablation on tumor promotion associated with FBXL5 deficiency were also observed in female mice (Fig. 1 B). This genetic evidence thus indicated that aberrant IRP2 activity in *Alb*-Cre/*Fbxl5*$^{F/F}$ mice is responsible for the tumor-promoting effect of FBXL5 ablation, with FBXL5 protecting the liver from carcinogenesis by suppressing IRP2 activity.

We next examined whether FBXL5 deficiency in the liver influences the survival of DEN-injected mice. The survival rate of male or female *Alb*-Cre/*Fbxl5*$^{F/F}$ mice was significantly

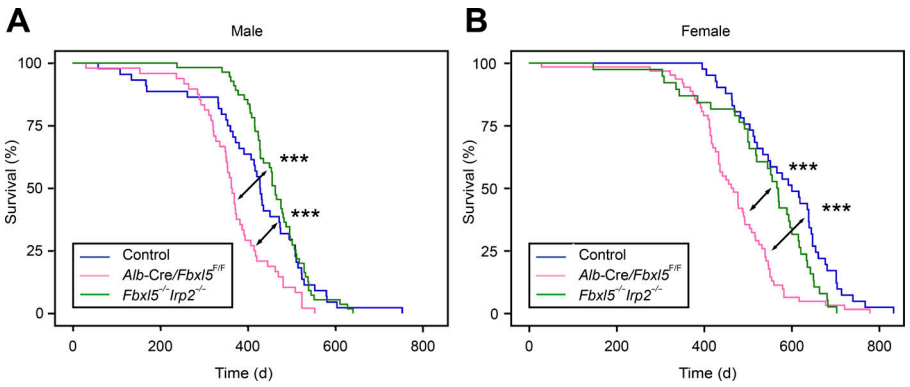

Figure 2. **FBXL5 deficiency is associated with poor survival of DEN-injected mice. (A)** Survival rate of DEN-injected *Fbxl5*$^{F/F}$ (n = 44), *Alb*-Cre/*Fbxl5*$^{F/F}$ (n = 48), or *Fbxl5*$^{-/-}$*Irp2*$^{-/-}$ (n = 55) male mice. ***, P < 0.005 (log-rank test). **(B)** Survival rate of DEN-injected *Fbxl5*$^{F/F}$ (n = 41), *Alb*-Cre/*Fbxl5*$^{F/F}$ (n = 62), or *Fbxl5*$^{-/-}$*Irp2*$^{-/-}$ (n = 38) female mice. ***, P < 0.005 (log-rank test).

reduced compared with that for control *Fbxl5*$^{F/F}$ mice, whereas that of *Fbxl5*$^{-/-}$*Irp2*$^{-/-}$ mice was similar to that for control mice (Fig. 2). These results thus showed that the poor prognosis of DEN-injected *Alb*-Cre/*Fbxl5*$^{F/F}$ mice is dependent on the accumulation of IRP2 that results from the lack of FBXL5-mediated degradation of this protein.

Hepatic FBXL5 deficiency elicits iron overload and oxidative stress

To determine whether cellular iron metabolism is dysregulated in both HCC and nontumor liver tissue of DEN-injected *Alb*-Cre/*Fbxl5*$^{F/F}$ mice, we examined the expression of IRP2 and its target proteins. Immunoblot analysis revealed that IRP2 accumulated in both nontumor liver tissue and HCC of *Alb*-Cre/*Fbxl5*$^{F/F}$ mice (Fig. 3 A). Consistent with this finding, expression of transferrin receptor 1 (TfR1), which is indicative of IRP2 activity, was also increased in nontumor liver tissue and HCC of the FBXL5-deficient mice compared with control *Fbxl5*$^{F/F}$ mice (Fig. 3 A). Staining for both ferrous iron (Fe^{2+}) and ferric iron (Fe^{3+}) revealed marked accumulation of cellular iron in the liver of DEN-injected *Alb*-Cre/*Fbxl5*$^{F/F}$ mice, with the extent of iron accumulation in HCC being less pronounced than that in nontumor tissue (Fig. 3 B) despite the higher level of TfR1 expression in HCC (Fig. 3 A). The rapid proliferation of cancer cells might result in dilution of cellular iron. Indeed, these observations are consistent with previous results showing that iron depletion is a hallmark of HCC (Terada and Nakanuma, 1989; Deugnier et al., 1993). Collectively, our findings thus suggested that cellular iron metabolism is dysregulated in both HCC and nontumor liver tissue of *Alb*-Cre/*Fbxl5*$^{F/F}$ mice.

We next examined whether cellular iron overload in DEN-injected *Alb*-Cre/*Fbxl5*$^{F/F}$ mice induces oxidative stress in the liver. RT and real-time PCR analysis revealed significant up-regulation of mRNAs for proteins related to the NRF2-mediated oxidative stress response—such as NADPH quinone oxidoreductase 1 (Nqo1), heme oxygenase 1 (Hmox1), glutathione S-transferase A1 (Gsta1), and metallothionein 2 (MT2)—in nontumor liver tissue of the FBXL5-deficient mice compared with that of control mice (Fig. 3 C). The abundance of Nqo1, Hmox1, and Gsta1 mRNAs was also increased in the tumors of *Alb*-Cre/*Fbxl5*$^{F/F}$ mice. The amounts of these mRNAs did not differ significantly between tumor and nontumor tissue of the *Alb*-Cre/*Fbxl5*$^{F/F}$ mouse liver, however, suggesting that a mechanism in addition to oxidative stress might increase the mutation rate of FBXL5-deficient tumor cells. This notion is consistent with the fact that sequencing analysis of human HCC and experimentally induced rat or mouse HCC has revealed that the NRF2 gene is commonly mutated in the region encoding the domain of the transcription factor that interacts with its negative regulator Keap1 (Guichard et al., 2012; Zavattari et al., 2015; Ngo et al., 2017). We also tested whether expression of Cre recombinase alone activates NRF2 target genes in the liver by examining DEN-injected male *Alb*-Cre/*Fbxl5*$^{F/+}$ and *Fbxl5*$^{F/F}$ mice. Expression of the NRF2 target genes for Hmox1 and Nqo1 was similar for the two genotypes (Fig. S2 C), suggesting that Cre recombinase alone does not directly affect NRF2 activity in the liver. We further confirmed that Hmox1 expression was up-regulated at the protein level in nontumor liver tissue and HCC of *Alb*-Cre/*Fbxl5*$^{F/F}$ mice (Fig. 3 A). These results thus suggested that oxidative stress is induced in the liver of *Alb*-Cre/*Fbxl5*$^{F/F}$ mice.

ROS levels detected with the cell-permeable reagent 2′,7′-dichlorodihydrofluorescein diacetate or by deposition of 4-hydroxy-2-nonenal did not differ significantly between FBXL5-deficient and control hepatocytes (data not shown), despite the significant activation of oxidative stress response genes apparent in the former (Fig. 3 C). We previously showed that acute dietary iron overload induces marked 4-hydroxy-2-nonenal deposition and massive cell death in the FBXL5-deficient mouse liver (Moroishi et al., 2011). The activation of ROS scavenger genes in the FBXL5-deficient liver in the absence of acute dietary iron overload might limit oxidative stress to a level below that detectable by this method. Our findings thus suggested that chronic iron-induced oxidative stress at even a moderate level in the FBXL5-deficient liver promotes carcinogenesis.

FBXL5 deficiency induces the DNA damage response and inflammation in the liver

To explore in more detail the mechanism by which cellular iron overload promotes liver carcinogenesis, we performed RNA sequencing (RNA-seq) analysis for liver tumors and corresponding nontumor tissue in DEN-injected control and *Alb*-Cre/*Fbxl5*$^{F/F}$ mice. Consistent with our RT and real-time PCR data (Fig. 3 C), gene set enrichment analysis (GSEA) of the RNA-seq data indicated that the expression of NRF2 target genes is increased in both HCC and nontumor tissue of the FBXL5-deficient liver

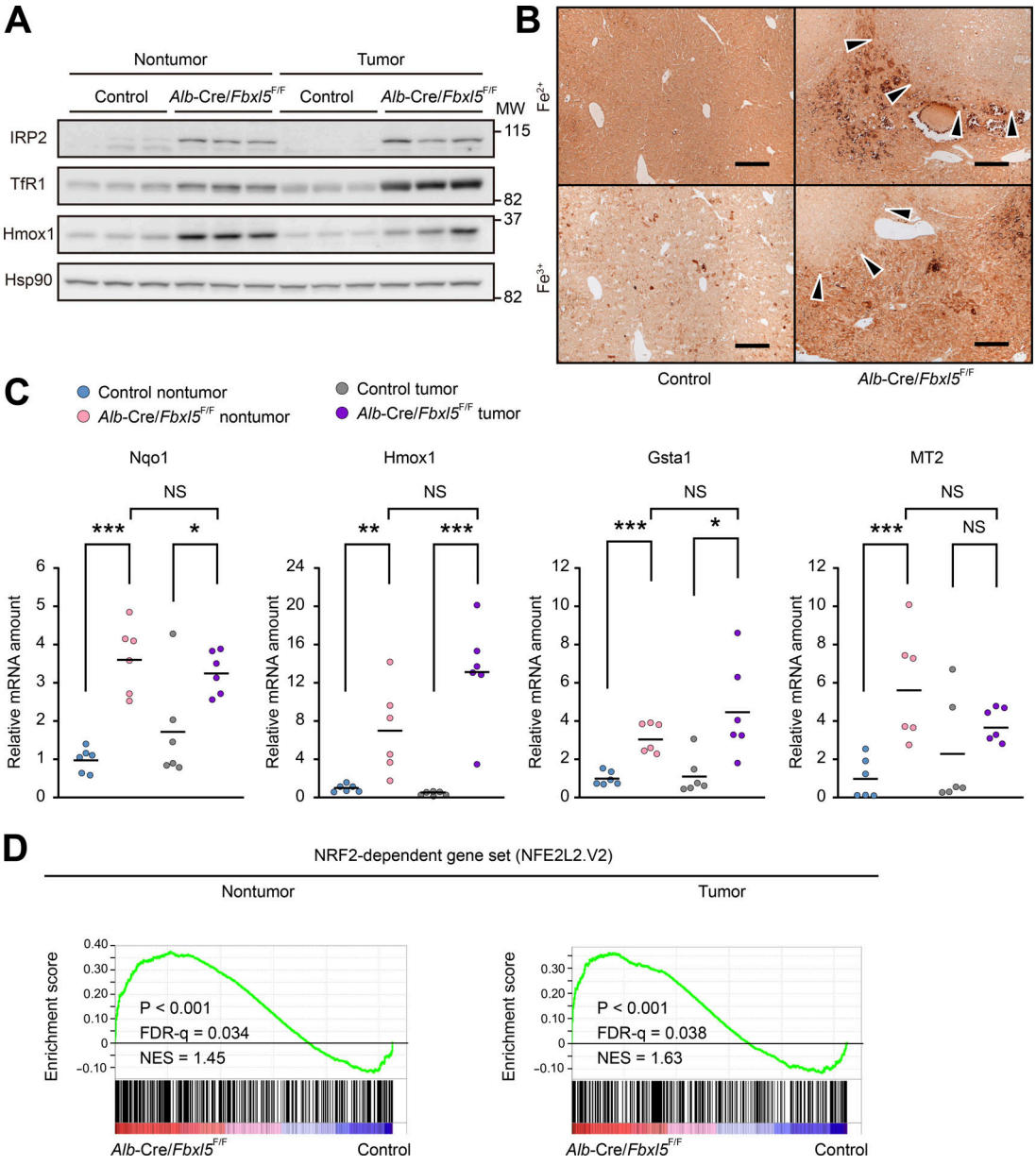

Figure 3. **FBXL5 deficiency disrupts iron and redox regulation in the liver. (A)** Immunoblot analysis of extracts of nontumor liver or HCC tissue from DEN-injected *Alb-Cre/Fbxl5*$^{F/F}$ or control *Fbxl5*$^{F/F}$ male mice (n = 3) at 36 wk of age with antibodies to IRP2, to TfR1, to Hmox1, or to Hsp90 (loading control). Representative blots of three independent experiments is shown. MW, molecular weight. **(B)** Diaminobenzidine-enhanced Turnbull or Perls staining for Fe^{2+} and Fe^{3+}, respectively, in the liver of DEN-injected *Fbxl5*$^{F/F}$ and *Alb*-Cre/*Fbxl5*$^{F/F}$ male mice at 36 wk of age. Arrowheads indicate a liver tumor. Bars, 200 µm. **(C)** RT and real-time PCR analysis of mRNAs for proteins related to oxidative stress in nontumor liver and HCC tissue of DEN-injected *Fbxl5*$^{F/F}$ (nontumor, n = 6; tumor, n = 6) and *Alb*-Cre/*Fbxl5*$^{F/F}$ (nontumor, n = 6; tumor, n = 6) male mice at 45 wk of age. Horizontal bars are means. *, P < 0.05; **, P < 0.01; ***, P < 0.005; NS (Student's t test). **(D)** GSEA plots of differentially expressed genes for the list of NRF2 target genes in a DEN-injected *Alb*-Cre/*Fbxl5*$^{F/F}$ male mice (nontumor, n = 5; tumor, n = 5) compared with two DEN-injected littermate control *Fbxl5*$^{F/F}$ male mice (nontumor, n = 6; tumor, n = 6) at 45 wk of age. FDR-q, false discovery rate q value; NES, normalized enrichment score.

compared with the control liver (Fig. 3 D), suggesting that oxidative stress is indeed increased by the loss of FBXL5. The induction of DNA damage by oxidative stress contributes to the accumulation of somatic mutations and carcinogenesis in the liver (Farazi and DePinho, 2006; Cichoż-Lach and Michalak, 2014). Indeed, GSEA suggested that the G_2-M checkpoint, the activation of which is a hallmark of the DNA damage response, is activated to a greater extent in FBXL5-deficient liver tumors than in control tumors (Fig. 4, A and B). Consistent with this finding, the number of somatic mutations found in tumor regions but not in nontumor liver tissue of the same animals was greater for *Alb*-Cre/*Fbxl5*$^{F/F}$ mice than for *Fbxl5*$^{F/F}$ mice (Fig. 4 C). These results confirmed that FBXL5 deficiency induces harmful oxidative stress and induction of the DNA damage response in the DEN-exposed liver.

A

Tumor

Hallmark gene set enriched in *Alb*-Cre/*Fbxl5*$^{F/F}$	NES	P	FDR-q
E2F_TARGETS	1.74	0.000	0.014
REACTIVE_OXYGEN_SPECIES_PATHWAY	1.71	0.002	0.010
G2M_CHECKPOINT	1.65	0.000	0.011
OXIDATIVE_PHOSPHORYLATION	1.63	0.000	0.011
MITOTIC_SPINDLE	1.60	0.000	0.014

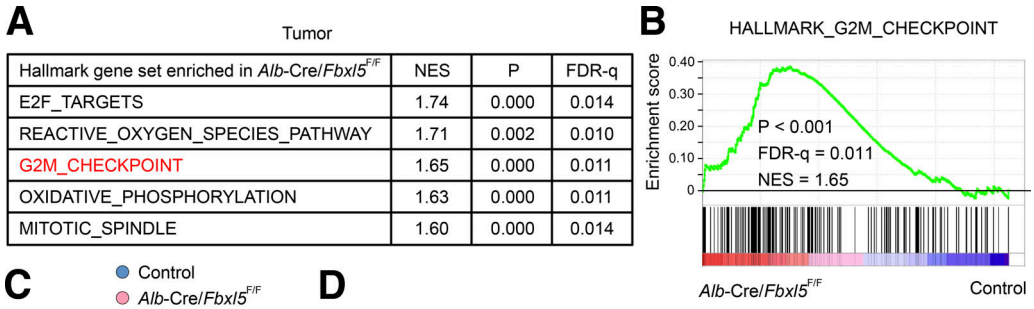

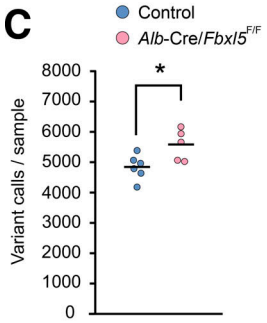

D

Nontumor

Hallmark gene set enriched in *Alb*-Cre/*Fbxl5*$^{F/F}$	NES	P	FDR-q
ALLOGRAFT_REJECTION	2.32	0.000	0.000
INFLAMMATORY_RESPONSE	2.27	0.000	0.000
KRAS_SIGNALING_UP	1.95	0.000	0.000
INTERFERON_GAMMA_RESPONSE	1.91	0.000	0.000
COMPLEMENT	1.91	0.000	0.000

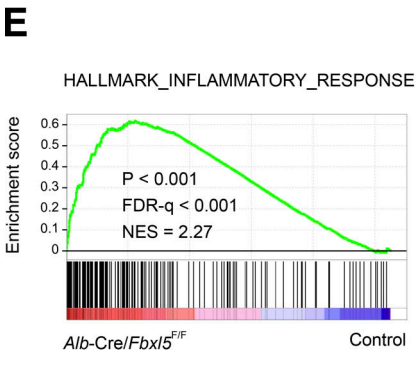

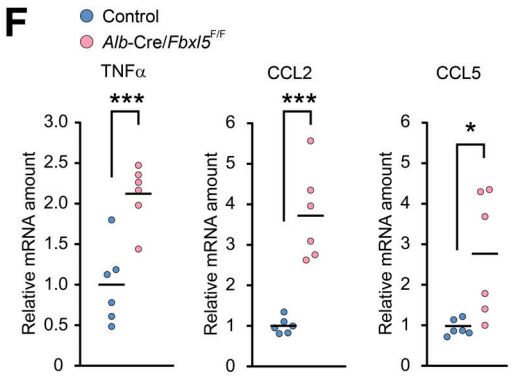

Figure 4. **Hepatic FBXL5 deficiency induces the DNA damage response and inflammation. (A and B)** GSEA of differentially expressed genes for hallmark gene sets (A) and the HALLMARK_G2M_CHECKPOINT gene set (genes related to the G_2-M checkpoint; B) in FBXL5-deficient hepatic tumors (n = 5) compared with control tumors (n = 6). **(C)** Somatic variants called with RNA-seq data for FBXL5-deficient hepatic tumors (n = 5) and control tumors (n = 6). Horizontal bars are means. *, P < 0.05 (Mann–Whitney U test). **(D and E)** GSEA of differentially expressed genes for hallmark gene sets (D) and the HALLMARK_INFLAMMATORY_RESPONSE gene set (genes related to the inflammatory response; E) in FBXL5-deficient (n = 5) compared with control (n = 6) nontumor liver tissue. **(F)** RT and real-time PCR analysis of mRNAs for proteins related to the inflammatory response in nontumor liver tissue of DEN-injected *Fbxl5*$^{F/F}$ (n = 6) and *Alb*-Cre/*Fbxl5*$^{F/F}$ (n = 6) male mice at 45 wk of age. Horizontal bars are means. *, P < 0.05; ***, P < 0.005 (Student's t test).

Oxidative stress or tissue damage induces inflammation in the liver, which in turn further promotes tissue damage and can lead to carcinogenesis (Farazi and DePinho, 2006). Consistent with this notion, GSEA revealed an augmented inflammatory response in the FBXL5-deficient liver (Fig. 4, D and E). RT and real-time PCR analysis also confirmed that the expression of genes for several inflammatory cytokines—including TNFα, C-C motif chemokine ligand 2 (CCL) 2, and CCL5—was increased in the liver of *Alb*-Cre/*Fbxl5*$^{F/F}$ mice (Fig. 4 F). These cytokines were all previously shown to contribute to hepatocarcinogenesis in mice (Knight et al., 2000; Li et al., 2017; Mohs et al., 2017). Together, these data indicated that hepatic FBXL5 deficiency induces toxic oxidative stress that promotes DNA damage and chronic inflammation in the liver.

Hepatic FBXL5 deficiency promotes liver damage and compensatory cell proliferation

Oxidative stress also promotes hepatocyte cell death and chronic liver damage (Kamata et al., 2005; Cichoż-Lach and Michalak, 2014).We investigated whether oxidative stress in the liver of *Alb*-Cre/*Fbxl5*$^{F/F}$ mice gives rise to tissue damage. The activity of alanine aminotransferase (ALT) in serum at 48 h after DEN injection at 15 d of age did not differ between *Alb*-Cre/*Fbxl5*$^{F/F}$ and control mice (Fig. 5 A), suggesting that acute DEN-induced hepatotoxicity as the initiating event of carcinogenesis was not exacerbated by FBXL5 deficiency. In contrast, serum ALT activity at 20 or 36 wk of age was significantly higher in *Alb*-Cre/*Fbxl5*$^{F/F}$ mice that had been injected with DEN at 15 d of age than in corresponding controls (Fig. 5 B), indicative of chronic liver damage in the FBXL5-deficient animals. Consistent with these findings, GSEA revealed increased expression of genes related to the cell death pathway activated in response to DNA damage in the FBXL5-deficient liver (Fig. 5 C). Chronic liver damage in hemochromatosis model mice has been associated with ferroptosis, a form of iron-dependent cell death (Dixon et al., 2012; Wang et al., 2017). To examine whether the liver damage in our FBXL5-deficient mice was related to ferroptosis, we monitored

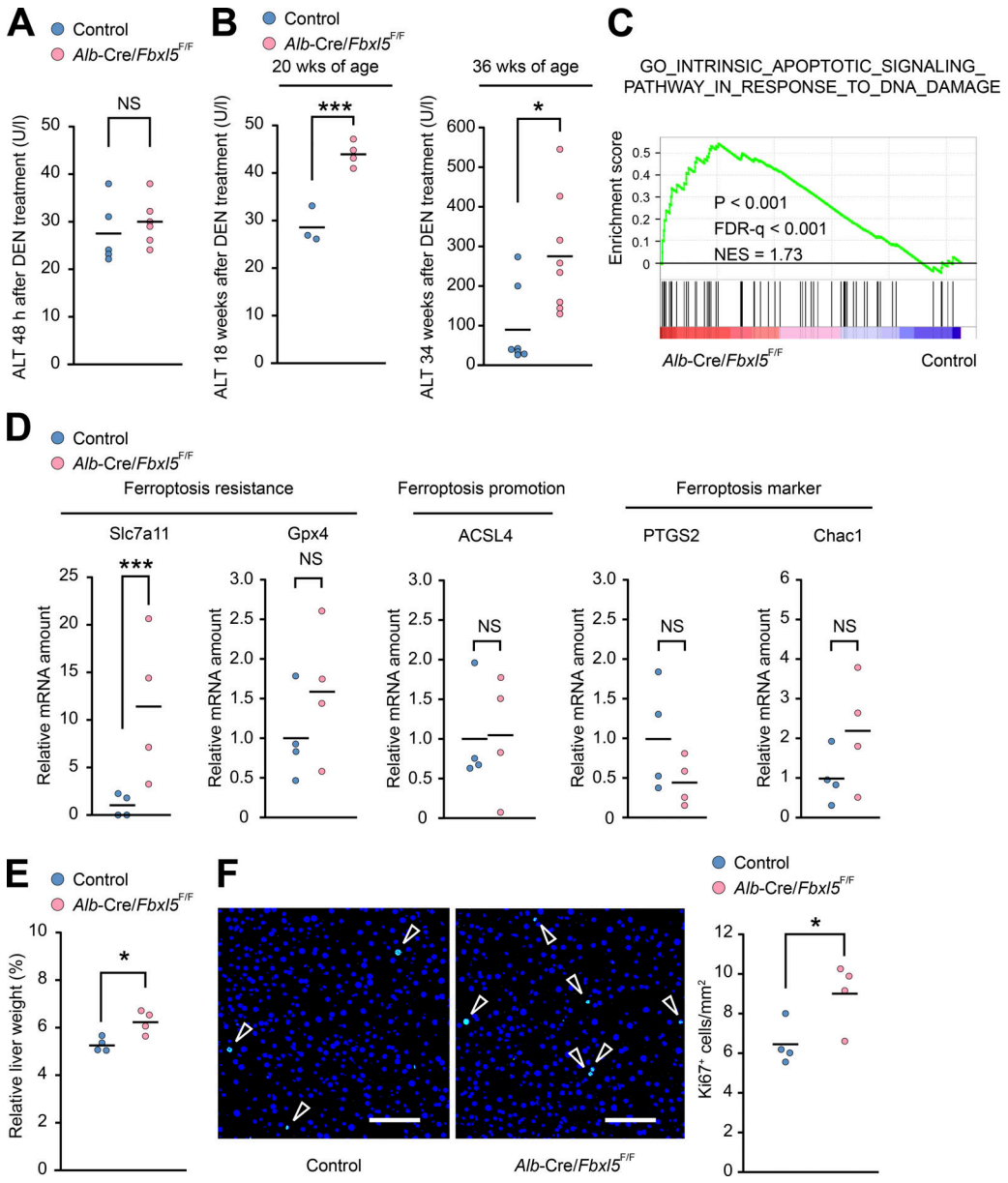

Figure 5. **FBXL5 deficiency induces liver damage and proliferation of hepatocytes. (A)** Serum ALT activity in *Fbxl5*$^{F/F}$ (n = 5) and *Alb*-Cre/*Fbxl5*$^{F/F}$ (n = 6) male mice at 48 h after DEN injection at 15 d of age. Horizontal bars are means. Statistical analysis was performed with the Student's t test. **(B)** Serum ALT activity in 20-wk-old *Fbxl5*$^{F/F}$ (n = 3) and *Alb*-Cre/*Fbxl5*$^{F/F}$ (n = 4) male mice (left) as well as in 36-wk-old *Fbxl5*$^{F/F}$ (n = 7) and *Alb*-Cre/*Fbxl5*$^{F/F}$ (n = 8) male mice (right) injected with DEN at 15 d of age. Horizontal bars are means. *, P < 0.05; ***, P < 0.005 (Student's t test). **(C)** GSEA plot of differentially expressed genes for the gene set related to cell death in response to DNA damage in FBXL5-deficient (n = 5) compared with control (n = 6) nontumor liver tissue. **(D)** RT and real-time PCR analysis of mRNAs for proteins associated with ferroptosis in total liver tissue of DEN-injected *Fbxl5*$^{F/F}$ (n = 4) and *Alb*-Cre/*Fbxl5*$^{F/F}$ (n = 4) male mice at 20 wk of age. Horizontal bars are means. ***, P < 0.005; NS (Student's t test). **(E)** Liver weight as a percentage of body weight for DEN-injected *Fbxl5*$^{F/F}$ (n = 4) and *Alb*-Cre/*Fbxl5*$^{F/F}$ (n = 4) male mice at 20 wk of age. Horizontal bars are means. *, P < 0.05; NS (Student's t test). **(F)** Immunofluorescence staining for Ki67 in liver sections and quantitation of Ki67-positive cells for DEN-injected *Fbxl5*$^{F/F}$ (n = 4) or *Alb*-Cre/*Fbxl5*$^{F/F}$ (n = 4) male mice at 20 wk of age. Ki67-positive cells were quantified in 13–16 random fields (0.41 mm^2/field) for each animal. Arrowheads indicate Ki67-positive cells. Bars, 100 µm. Horizontal bars are means. *, P < 0.05; NS (Student's t test).

the expression of genes associated with defense against (*Slc7a11* and *Gpx4*) or promotion of (*Acsl4*) this form of cell death as well as that of ferroptosis marker genes (*Ptgs2* and *Chac1*) in the liver at 20 wk of age (Yang et al., 2014; Chen et al., 2017; Doll et al., 2017). Whereas the abundance of *Slc7a11* mRNAs was highly up-regulated in the liver of *Alb*-Cre/*Fbxl5*$^{F/F}$ mice, the expression of ferroptosis marker genes was not significantly altered in the liver of these mice (Fig. 5 D). These results indicated that the oxidative damage apparent in the FBXL5-deficient liver is not directly associated with ferroptosis, possibly as a result of the activation of antiferroptotic gene expression in response to chronic iron overload or oxidative stress.

The regenerative proliferation of hepatocytes that occurs in response to chronic liver damage has been shown to promote

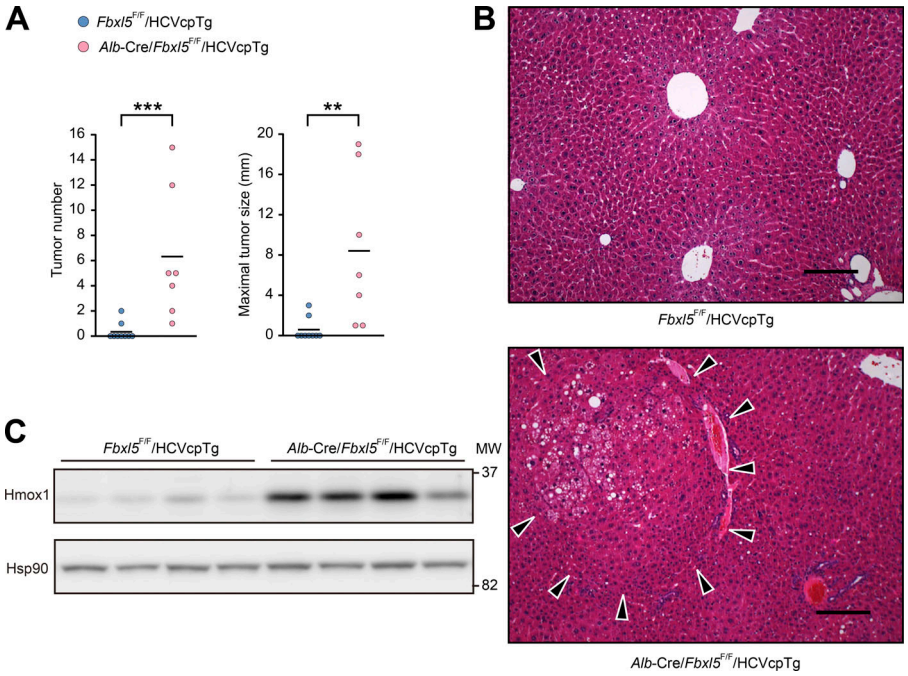

Figure 6. **FBXL5 deficiency promotes liver carcinogenesis induced by HCV core protein.** **(A)** Tumor multiplicity and maximal tumor diameter in the liver of *Fbxl5*$^{F/F}$/HCVcpTg (n = 9) or *Alb*-Cre/*Fbxl5*$^{F/F}$/HCVcpTg (n = 7) male mice at 90 wk of age. Horizontal bars are means. **, P < 0.01; ***, P < 0.005 (Mann–Whitney U test). **(B)** Hematoxylin-eosin staining of liver sections from *Fbxl5*$^{F/F}$/HCVcpTg or *Alb*-Cre/*Fbxl5*$^{F/F}$/HCVcpTg male mouse littermates at 90 wk of age. Arrowheads indicate a liver tumor. Bars, 200 µm. **(C)** Immunoblot analysis of liver extracts from 90-wk-old *Fbxl5*$^{F/F}$/HCVcpTg or *Alb*-Cre/*Fbxl5*$^{F/F}$/HCVcpTg male mice (n = 4) with antibodies to Hmox1 and to Hsp90. Representative blots of two independent experiments is shown. MW, molecular weight.

liver carcinogenesis (Maeda et al., 2005; Luedde et al., 2014; Marquardt et al., 2015). Our observation that the weight of the FBXL5-deficient liver was greater than that of the control liver, despite the apparent absence of tumor formation, at 20 wk of age (Fig. 5 E) suggested that the regenerative proliferation of hepatocytes might be induced in the liver of FBXL5-deficient mice. Indeed, we found that the frequency of proliferative (Ki67-positive) hepatocytes in DEN-injected *Alb*-Cre/*Fbxl5*$^{F/F}$ mice at 20 wk of age was greater than that in corresponding controls (Fig. 5 F). These observations thus suggested that FBXL5 deficiency results in chronic hepatocellular damage and proliferation of hepatocytes.

FBXL5 deficiency promotes carcinogenesis induced by HCV core protein

To test the generality of the effect of FBXL5 deficiency on liver carcinogenesis, we next examined a mouse model of carcinogenesis induced by expression of a transgene for HCV core protein (HCVcpTg mice; Moriya et al., 1998). The number and size of liver tumors formed in *Alb*-Cre/*Fbxl5*$^{F/F}$/HCVcpTg mice were significantly increased compared with those for *Fbxl5*$^{F/F}$/HCVcpTg control mice (Fig. 6 A). Histopathologic analysis of hepatic tissue sections confirmed these findings (Fig. 6 B). Immunoblot analysis also showed that Hmox1 accumulated to a greater extent in the liver of *Alb*-Cre/*Fbxl5*$^{F/F}$/HCVcpTg mice than in that of *Fbxl5*$^{F/F}$/HCVcpTg mice (Fig. 6 C), suggesting that FBXL5 deficiency also exacerbated oxidative stress in the liver of HCVcpTg mice. Together, these data indicated that the tumor-promoting effect of FBXL5 deficiency in the liver is not limited to chemically induced HCC but is also operative in a model of virus-induced HCC.

FBXL5 deficiency is associated with poor prognosis in human HCC patients

Our mouse data indicated that cellular iron dysregulation induced by FBXL5 deficiency promotes liver carcinogenesis and thereby shortens survival time. Given that FBXL5 mRNA was previously shown to be down-regulated in the liver of patients with viral hepatitis (Nanba et al., 2016), we examined whether reduced expression of *FBXL5* is associated with a poor prognosis in human HCC with The Cancer Genome Atlas (TCGA) Liver Hepatocellular Carcinoma (LIHC) dataset (Cerami et al., 2012; Gao et al., 2013) or data accessed at the Gene Expression Omnibus (GEO) database with the tag GSE14520 (Roessler et al., 2010). Patients in the TCGA-LIHC cohort were subdivided into quartile groups on the basis of *FBXL5* expression level, and their survival was compared with Kaplan–Meier plots. The group with the lowest 25% of *FBXL5* expression level showed the shortest survival and was thus considered the most clinically important among the quartile groups (Fig. 7 A and Fig. S3 A). Consistent with this finding, the group with the lowest 25% of *FBXL5* expression level in the GSE14520 dataset also had a poorer prognosis compared with the group with the highest 75% (Fig. 7, B and C). Furthermore, the group with the lowest 25% of *FBXL5* expression level in the TCGA-LIHC cohort harbored more somatic mutations than did the group with the highest 75% (Fig. S3 B). The abundance of TfR1 mRNA, which is up-regulated by IRP2 and therefore represents an index of IRP2 activity, was also increased in HCC patients with a low *FBXL5* expression level (Fig. 7 D). Furthermore, GSEA showed that genes whose expression was down-regulated in cultured cells by knockdown of TfR1 were significantly activated in HCC with a low level of *FBXL5* expression (Fig. 7 E), suggesting that the up-regulation of TfR1 mRNA in HCC with a low *FBXL5* expression level had functional consequences. GSEA also showed that marker genes whose expression is up-regulated in proliferative HCC and genes highly expressed in HCC with a poor prognosis were significantly associated with a low level of *FBXL5* expression in HCC (Fig. 7, F and G). *FBXL5* expression was found to be significantly down-regulated in HCC associated with hemochromatosis

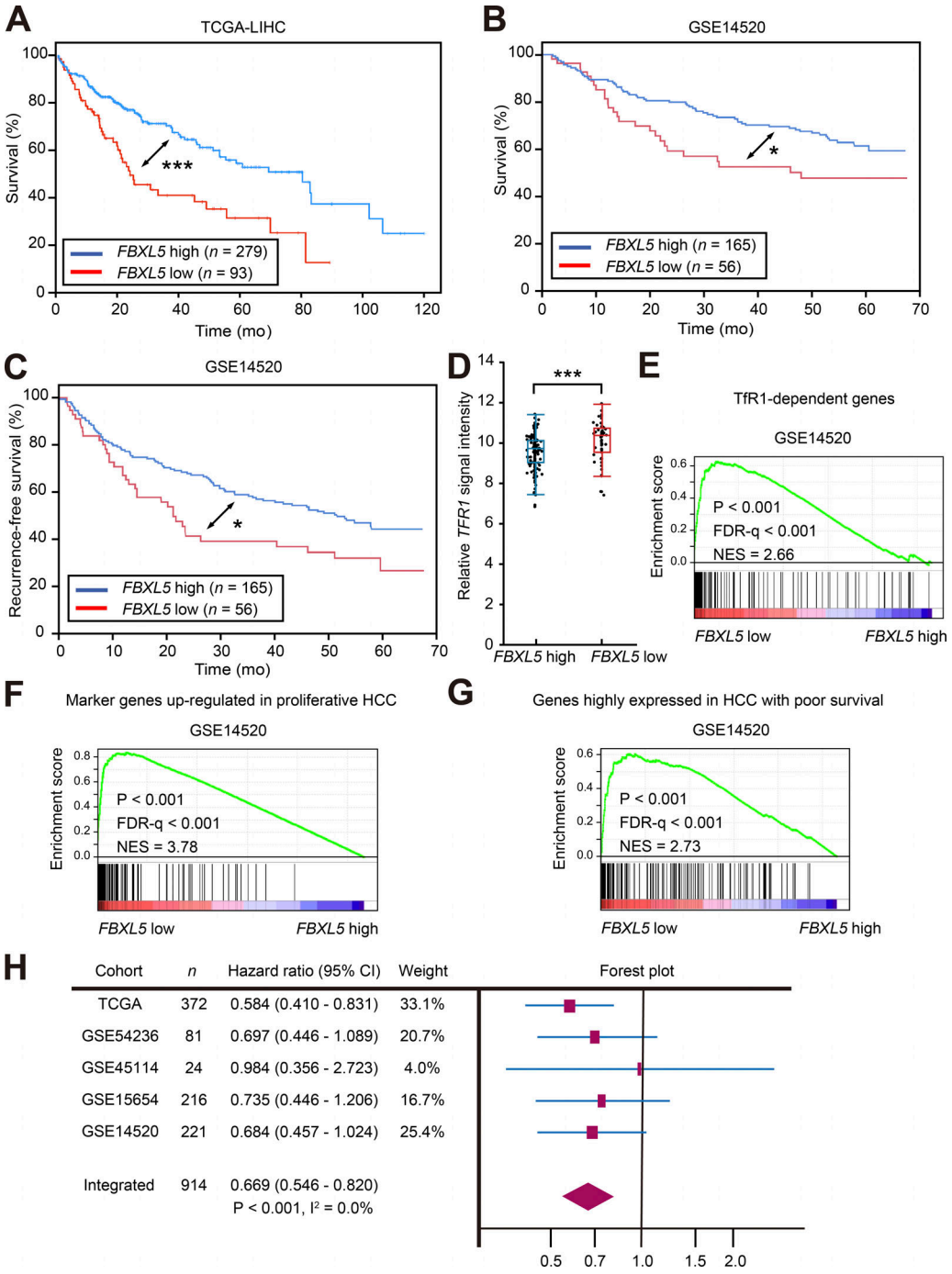

Figure 7. **Down-regulation of *FBXL5* expression is associated with poor prognosis of human HCC. (A)** Survival curves for HCC patients with high (n = 279) or low (n = 93) levels of *FBXL5* expression were constructed from TCGA-LIHC dataset. ***, P < 0.005 (log-rank test). **(B)** Survival curves for HCC patients with high (n = 165) or low (n = 56) levels of *FBXL5* expression were constructed from the GSE14520 dataset. *, P < 0.05 (log-rank test). **(C)** Recurrence-free survival for the HCC patients with high (n = 165) or low (n = 56) levels of *FBXL5* expression in the GSE14520 dataset. *, P < 0.05 (log-rank test). **(D)** Relative TfR1 mRNA signal intensity for HCC with high (n = 165) or low (n = 56) levels of *FBXL5* expression in the GSE14520 dataset. Box-and-whisker plots show median, interquartile range, and most extreme data point less than 1.5 interquartile range from box. ***, P < 0.005 (Student's t test). **(E–G)** GSEA plots of differentially expressed genes in HCC with high (n = 165) or low (n = 56) levels of *FBXL5* expression (GSE14520 dataset) for the list of genes down-regulated in P493-6 cells in response to knockdown of TfR1 mRNA (E), for the list of marker genes whose expression is up-regulated in proliferative HCC (F), or for the list of genes highly expressed in HCC with poor prognosis (G). **(H)** Meta-analysis and forest plot of the hazard ratio and 95% CI for the association between *FBXL5* expression and overall survival in HCC patients (n = 914) of five different cohorts according to the random effects model.

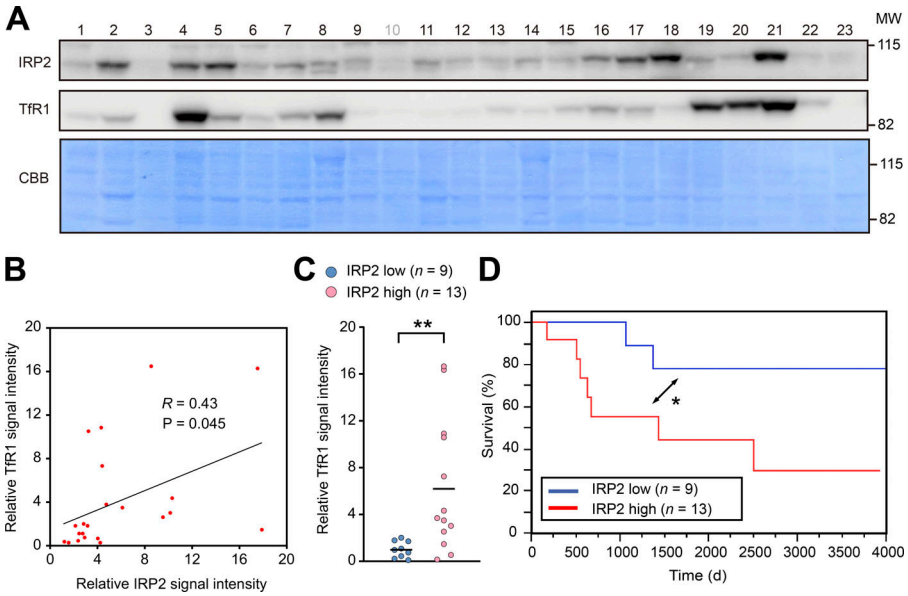

Figure 8. **Accumulation of IRP2 is associated with poor prognosis of human HCC. (A)** Immunoblot analysis of IRP2 and TfR1 in extracts prepared from surgical specimens of human HCC. The membrane was also stained with Coomassie Brilliant Blue (CBB) as a loading control. Specimen 10 was excluded from subsequent analysis because of the HCC-unrelated death of the patient within 3 mo after surgery. MW, molecular weight. **(B)** Correlation of IRP2 and TfR1 protein abundance in the HCC specimens (n = 22). R, Pearson's correlation coefficient. **(C)** TfR1 protein abundance in the HCC specimens with low (n = 9) or high (n = 13) IRP2 protein expression. Each point represents an individual specimen, with the horizontal lines indicating mean values. **, P < 0.01 (Mann–Whitney U test). **(D)** Survival curves for the HCC patients with a low (n = 9) or high (n = 13) IRP2 abundance. *, P < 0.05 (log-rank test).

compared with HCC associated with chronic viral hepatitis (Fig. S4), suggesting that loss of *FBXL5* expression might play a greater role in liver carcinogenesis in patients with hemochromatosis. To reinforce the connection between our mouse data and human HCC, we retrieved an additional three human HCC trancriptomic datasets from the Array Express archive of the European Bioinformatics Institute (EBI). These datasets and the TCGA-LIHC dataset together include clinical data for a total of 914 patients. Meta-analysis of these five HCC cohorts revealed that the prognosis of the group with the lower 50% of *FBXL5* expression level had a significantly poorer prognosis than did that with the higher 50% (hazard ratio, 0.665; P < 0.001; Fig. 7 H). Given that meta-analysis is one of the most reliable methods in medical statistics, we conclude that a low *FBXL5* expression level is indeed strongly associated with poor prognosis in human HCC, although further investigations are still needed to validate our correlative findings based on published human data.

Given that FBXL5 deficiency resulted in an increase in the amounts of IRP2 and TfR1 proteins in the liver of mice (Fig. 3 A), we postulated that IRP2 protein abundance might also be associated with a poor clinical outcome in human HCC. To examine this possibility, we analyzed surgical specimens of human HCC for the expression of IRP2 and TfR1 (Fig. 8 A). The expression level of IRP2 was largely correlated with that of TfR1 in the HCC specimens (Fig. 8, B and C), suggesting that an increase in IRP2 abundance results in up-regulation of TfR1 at the posttranscriptional level in most tumors. Finally, a high level of IRP2 protein expression was associated with a worse prognosis compared with a low level of IRP2 expression in these HCC patients (Fig. 8 D). Collectively, our findings thus implicate the cellular iron overload that results from FBXL5 down-regulation and consequent IRP2 accumulation in the exacerbation of HCC in mice and possibly in humans (Fig. 9).

Discussion

We have here uncovered a previously unrecognized role of cellular iron homeostasis governed by FBXL5 in defense against oxidative stress and hepatocarcinogenesis with the use of mouse models of conditional *Fbxl5* deletion. Mechanistically, disruption of FBXL5-mediated cellular iron homeostasis results in iron overload and consequent oxidative stress in the liver of mice exposed to chemical or viral carcinogens. Iron-induced oxidative stress in such mice triggers liver damage, inflammation, and compensatory proliferation of hepatocytes, eventually leading to hepatocarcinogenesis. Analysis of public datasets revealed that down-regulation of *FBXL5* expression was associated with poor prognosis of HCC patients. Additional ablation of IRP2 in conditional FBXL5-deficient mice prevented the promotion of hepatic carcinogenesis and improved survival, suggesting that IRP2 might be a potential therapeutic target for the prevention or treatment of liver cancer associated with down-regulation of *FBXL5* expression.

Our finding that tumor incidence in DEN-injected FBXL5-deficient mice is much greater than that in littermate controls (Fig. S1 and Fig. 6 A) suggested that hepatic tumors in the former mice are likely initiated earlier than those in the latter. The number of tumors in both DEN and HCV models was also greater for FBXL5-deficient mice than for control mice (Fig. 1 B, Fig. 6 A, and Fig. S1), suggesting that FBXL5 deficiency mainly affects tumor initiation rather than growth. Given that hepatic FBXL5 ablation alone essentially does not induce carcinogenesis, FBXL5 deficiency may promote the generation of tumor cells by accelerating the accumulation of mutations (Fig. 4, A–C). Dysregulation of FBXL5 may thus not be the cause (initiator) of carcinogenesis by itself but rather a risk factor for poor prognosis (promoter) in HCC. We therefore conclude that liver-specific FBXL5-deficient mice are a clinically relevant model for studies of HCC associated with hepatic iron overload.

FBXL5 is a master regulator of cellular iron metabolism by virtue of its role as the substrate recognition component of the SCF^{FBXL5} E3 ubiquitin ligase complex for IRP2 degradation (Salahudeen et al., 2009; Vashisht et al., 2009). Other proteins targeted by FBXL5 for proteasomal degradation include $p150^{Glued}$ and single-stranded DNA binding protein 1 (Zhang

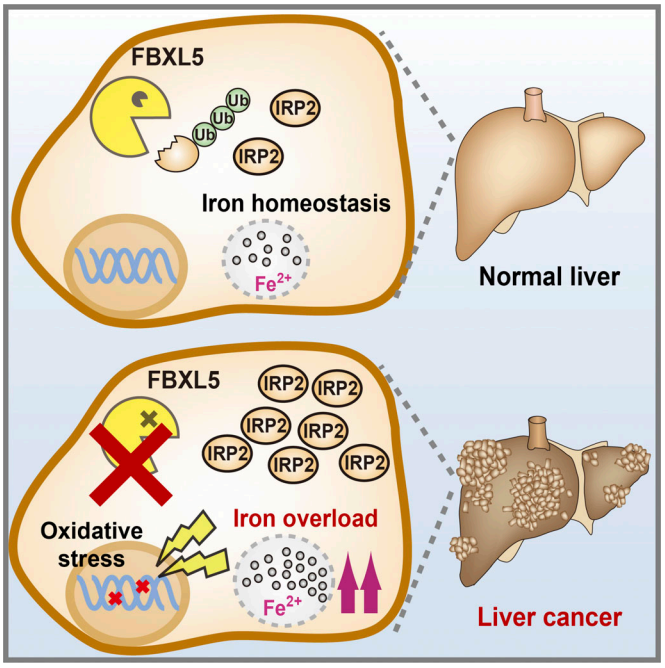

Figure 9. **Proposed model for the promotion of liver cancer by FBXL5 down-regulation and consequent IRP2 accumulation and iron overload.** Cellular iron homeostasis in the liver is governed by the FBXL5–IRP2 axis. FBXL5 deficiency in the liver results in cellular iron overload as a result of IRP2 overactivity. Cellular iron overload promotes oxidative stress, which leads to lipid peroxidation and oxidative damage to cellular membranes and macromolecules including DNA. Down-regulation of *FBXL5* gene expression and IRP2 protein accumulation in HCC is associated with poor prognosis. Ub, ubiquitin.

et al., 2007; Chen et al., 2014). FBXL5 has also been shown to interact with and to trigger the degradation of Snail1 (Viñas-Castells et al., 2014; Wu et al., 2015) and CBP/p300-interacting transactivator 2 (CITED2; Machado-Oliveira et al., 2015). Snail1 was found to induce epithelial-to-mesenchymal transition and to confer characteristics of tumor-initiating stem cells in a human HCC cell line (Dang et al., 2011). This observation suggests that the accumulation of Snail1 might also contribute to the promotion of carcinogenesis in the FBXL5-deficient liver. In contrast, CITED2 was shown to down-regulate the expression of cyclin D1, telomerase reverse transcription, and matrix metallopeptidase 2 as well as to suppress the proliferation of a human HCC cell line (Cheung et al., 2013). However, our data provide genetic evidence that IRP2 accumulation is largely responsible for the promotion of HCC by FBXL5 ablation, given that the enhancement of tumorigenesis in the FBXL5-deficient liver was prevented by additional ablation of IRP2. This latter result suggests that any contribution of Snail1 or CITED2 to tumorigenesis in the FBXL5-deficient liver is limited. We therefore conclude that FBXL5 plays an essential role in the defense against hepatocarcinogenesis through suppression of IRP2 activity.

Our results show that FBXL5 ablation in the liver results in promotion of carcinogenesis through cellular iron overload. Disruption of systemic iron homeostasis leads to iron deposition in various organs including the liver and promotes the development of liver cancer in patients with primary or secondary hemochromatosis (Bacon et al., 2011), although disruption of cellular iron homeostasis has not previously been shown to promote liver carcinogenesis. We now demonstrate for the first time that cellular iron homeostasis is essential for suppression of liver carcinogenesis. Furthermore, the amount of Fe^{2+}, rather than that of Fe^{3+}, is primarily increased in FBXL5-deficient liver tissue (Moroishi et al., 2011), suggesting that Fe^{2+} specifically has a cancer-promoting effect. This notion is consistent with the fact that Fe^{2+} is unstable and readily participates in the Fenton reaction, resulting in the uncontrolled production of the hydroxyl radical. Selective chelation of intracellular Fe^{2+} in the liver or HCC tissue might thus be a more effective treatment than the systemic Fe^{3+} chelation therapy or phlebotomy currently administered in some HCC patients. Indeed, we propose that the FBXL5–IRP2 axis is a potentially valuable therapeutic target for human HCC.

We also show that FBXL5 is an essential regulator of ROS in the liver as a result of its function in cellular iron regulation. The expression of several genes that contribute to oxidative stress responses was up-regulated in FBXL5-deficient HCC or non-tumor liver tissue, indicative of iron-mediated cellular damage and disruption of redox homeostasis. These genes included *Nqo1*, *Hmox1*, *Mt2*, and *Slc7a11*, the last of which encodes a component of system xc(−). System xc(−) contributes to the maintenance of cellular redox homeostasis by mediating the import of cystine for synthesis of the major cellular antioxidant glutathione. Inhibition of system xc(−) by erastin in cancer cells triggers ferroptosis, a recently recognized form of iron-dependent cell death (Dixon et al., 2012). Up-regulation of *Slc7a11* expression might therefore represent a mechanism to protect cells with cellular iron overload from ferroptosis. Indeed, *SLC7A11* is highly expressed in human tumors including liver cancer, and its overexpression inhibits ROS-induced ferroptosis in xenograft models of human cancer (Jiang et al., 2015). Marked up-regulation of *Slc7a11* expression in the FBXL5-deficient liver might suppress ferroptosis, which has been detected in hemochromatosis model mice (Wang et al., 2017). This substantial activation of genes associated with protection against ferroptosis might contribute to the promotion of carcinogenesis in the FBXL5-deficient animals. *Nqo1*, *Slc7a11*, *Hmox1*, and *Mt2* are also well-characterized oxidative stress response genes whose expression is regulated by the transcription factor NRF2, suggesting that oxidative stress induces NRF2 activation in the FBXL5-deficient liver and HCC. Expression of NRF2 was previously shown to be up-regulated in human HCC and to be correlated with tumor differentiation, metastasis, and size as well as associated with a poor prognosis (Zhang et al., 2015). Furthermore, NRF2 was recently shown to be essential for hepatocarcinogenesis in DEN-injected mice (Ngo et al., 2017), suggesting that constitutive activation of NRF2 target genes also contributes to the progression of liver cancer in *Alb*-Cre/*Fbxl5*$^{F/F}$ mice. These lines of evidence suggest that iron-dependent NRF2 activation might also contribute to the progression of HCC in the FBXL5-deficient liver.

Analysis of public datasets revealed that down-regulation of *FBXL5* expression was associated with poor prognosis in HCC

patients. However, no specific mutation in the *FBXL5* gene has been found to be associated with HCC or mode of tumorigenesis. Although the regulation of FBXL5 expression remains largely unclear, mutations in the *KDM5C* gene for a histone H3 lysine-4 demethylase were found to induce loss of DNA methylation at the *FBXL5* promoter in human samples (Grafodatskaya et al., 2013). The level of DNA methylation at the *FBXL5* gene in human blood was also found to be correlated with the abundance of KDM5C, suggesting that the amount of FBXL5 mRNA might be regulated by KDM5C. Furthermore, KDM5C was shown to be abundantly expressed in invasive human HCC cells, and depletion of KDM5C by RNA interference inhibited HCC cell migration, invasion, and epithelial–mesenchymal transition in vitro (Ji et al., 2015). Collectively, these observations suggest that FBXL5 expression might be regulated at the epigenetic level, although further studies are required to verify this notion.

Our finding that suppression of aberrant IRP2 activity prevented the promotion of hepatocarcinogenesis induced by FBXL5 ablation suggests that targeting of IRP2 might be effective for mitigation of hepatocellular iron overload and therefore a candidate for therapeutic application. This notion is further supported by the finding that the abundance of IRP2 protein was correlated with that of TfR1 protein in human HCC, with increased IRP2 expression also being associated with reduced survival of HCC patients. Given that complete loss of IRP2 gives rise to microcytic anemia or neurodegeneration in mice (Cooperman et al., 2005; Galy et al., 2005), however, an appropriate level of IRP2 suppression would be needed for clinical benefit. Another potential limitation of such a therapeutic strategy is that no IRP2 inhibitor has been developed to date. Given that IRP2 is an mRNA binding protein, inhibition of such binding with antisense oligonucleotides might be a feasible approach to the treatment of HCC associated with FBXL5 down-regulation and cellular iron overload, although further studies will be necessary to validate the connection between FBXL5 down-regulation and human HCC.

Materials and methods

Mice

Generation of *Fbxl5*$^{F/F}$ and *Fbxl5*$^{+/-}$ mice was described previously (Moroishi et al., 2011). These mice were crossed with *Alb*-Cre transgenic mice (Postic and Magnuson, 2000), *Irp2*$^{-/-}$ mice (LaVaute et al., 2001), or HCVcpTg mice (Moriya et al., 1998) to generate *Alb*-Cre/*Fbxl5*$^{F/F}$, *Fbxl5*$^{-/-}$*Irp2*$^{-/-}$, or *Alb*-Cre/*Fbxl5*$^{F/F}$/HCVcpTg mice. For chemically induced liver carcinogenesis, a single dose (25 mg/kg) of DEN (Sigma-Aldrich) was injected i.p. in mice at 15 d of age (Sarma et al., 1986). The injected mice were analyzed at 36 wk of age unless indicated otherwise. *Alb*-Cre/*Fbxl5*$^{F/F}$/HCVcpTg or *Fbxl5*$^{F/F}$/HCVcpTg mice were analyzed at 90 wk of age. Externally visible tumors (>1 mm in diameter) were counted and measured. All mice were maintained on a mixed genetic background (C57BL/6;129/Sv), and all mouse experiments were approved by the Animal Ethics Committee of Kyushu University.

Human specimens

Tissue specimens were obtained from 23 male patients with liver tumors who underwent hepatectomy at the Department of Gastroenterological Surgery, Osaka University Hospital (Table S1). The specimens were frozen immediately in liquid nitrogen and stored at −80°C for subsequent immunoblot analysis. The signal intensities of immunoblot bands were quantified with ImageJ software (National Institutes of Health). Specimen 10 was excluded from quantitative analysis because of the HCC-unrelated death of the patient within 3 mo after surgery. The cutoff value for classification of IRP2 expression level as high or low was determined with the minimal P value approach (Budczies et al., 2012; Hirata et al., 2016). The study protocol was approved by the Human Ethics Review Committees of Osaka University and Kyushu University, and a signed consent form was obtained from each patient for the use of tissue samples for medical research.

Analysis of published data

Overall survival was compared between HCC patients with high or low levels of *FBXL5* expression in the TCGA-LIHC dataset accessed with cBioPortal (Cerami et al., 2012; Gao et al., 2013). Overall survival and recurrence-free survival were also compared between HCC patients with high or low *FBXL5* expression levels with data accessed at GEO with the tag GSE14520 (Roessler et al., 2010). The data processed on the 96 HT HG-U133A 2.0 microarray platform were downloaded as a series matrix file and analyzed. The signal intensities for *FBXL5* (209004_s_at) were then collated with those for *TFR1* (208691_at) or the survival data included in the supplementary file "GSE14520_Extra_Supplement.txt.gz" downloaded from GEO. Survival curves were generated with the use of library ggplot2 in the R package (Fig. 7 A and Fig. S3 A) or JMP software (SAS Institute; Fig. 7, B and C). Normalized expression data accessed at GEO with the tag GSE14520 and used for the survival analysis in Fig. 7 B were then analyzed with GSEA v2.0.13 software (Broad Institute) and the ODONNELL_TFRC_TARGETS_DN (Fig. 7 E), CHIANG_LIVER_CANCER_SUBCLASS_PROLIFERATION_UP (Fig. 7 F) and LEE_LIVER_CANCER_SURVIVAL_DN (Fig. 7 G) gene sets. These gene sets were obtained from the Molecular Signatures Database v4.0 distributed at the GSEA web site. Patients were grouped on the basis of the abundance of FBXL5 mRNA, with the upper 75% and lower 25% representing the high and low expression groups, respectively (Fig. 7, A–G; and Fig. S3 B). For the meta-analysis in Fig. 7 H, we retrieved the TCGA-LIHC dataset from cBioPortal as well as four human HCC trancriptomic datasets from the Array Express archive of EBI, and patients were grouped on the basis of the median value of FBXL5 mRNA abundance. We retrieved the mutation data in Fig. S3 B from cBioPortal. The signal intensity for *FBXL5* (209004_s_at) in HCC for patients with HBV infection, HCV infection, or hemochromatosis was analyzed with the E-MTAB950 dataset from the Array Express archive of EBI (Fig. S4).

RNA-seq analysis

Total RNA was extracted from nontumor and tumor tissue of a DEN-injected *Alb*-Cre/*Fbxl5*$^{F/F}$ male mouse (nontumor, n = 5; tumor, n = 5) and two DEN-injected littermate control *Fbxl5*$^{F/F}$ male mice (nontumor, n = 6; tumor, n = 6) at 45 wk of age with the use of a TRIzol Plus RNA Purification Kit (Life Technologies). Libraries were prepared with the use of a NEBNext Ultra

Directional RNA Library Prep Kit for Illumina. RNA-seq was performed as described previously (Katayama et al., 2016). Complementary DNA was sequenced with a HiSeq 2500 system (Illumina). The total amount of each transcript was calculated with the use of a series of programs including TopHat2 and Cufflinks. RNA-seq reads were mapped against the mouse (mm10) genome. Normalized expression data were then analyzed with GSEA v2.0.13 software (Broad Institute) and Hallmark (Fig. 4, A, B, D, and E), NFE2L2.V2 (Fig. 3 D), and GO_INTRINSIC_APOPTOTIC_SIGNALING_PATHWAY_IN_RESPONSE_TO_DNA_DAMAGE (Fig. 5 C) gene sets obtained from the Molecular Signatures Database v4.0 distributed at the GSEA Web site.

Variant calling for RNA-seq data

Somatic variant calling was performed largely based on the previously reported pipeline for processing of RNA-seq data from tumor samples in order to identify somatic mutations with the use of MuTect2 (McKenna et al., 2010; Coudray et al., 2018). The use of MuTect2 in somatic variant calling from RNA-seq data was also described by another group (Neums et al., 2018). After trimming the adapters (TrimGalore, v0.5.0) from fastq files, the data were aligned with STAR aligner (v2.4.2a) with the use of a two-pass procedure (Dobin and Gingeras, 2015). The aligned reads in BAM format were sorted, and duplicate reads were flagged (MarkDuplicates, Picard v2.5.0). RNA-seq reads were split into exons (SplitNCigarReads, GATK v3.6). Variant calling was then performed with MuTect2 (Cibulskis et al., 2013) in tumor versus normal mode, and variants recovered in VCF files were counted. Variant calling for each tumor sample was performed with all replicates of the corresponding mouse nontumor liver tissue, and the average of the count of variant calls is shown for each tumor in Fig. 4 C.

Histopathology and immunostaining

Liver tissue was fixed with 4% paraformaldehyde in PBS, embedded in paraffin, and sectioned at a thickness of 3 µm. Sections were stained with hematoxylin-eosin or immunostained with antibodies to Ki67 (550609; BD Biosciences). Immune complexes were detected with Alexa Fluor 488–conjugated goat secondary antibodies (Invitrogen; Li et al., 2004; Yokobori et al., 2009), and confocal images were acquired with an LSM 700 Laser Scanning Microscope (Carl Zeiss).

Iron histochemistry

The mouse liver was perfused with 50 mM hydrogen sulfide in deionized water and with 4% paraformaldehyde in PBS. Iron was detected in cryostat sections of the liver by enhanced Perls or Turnbull staining. Tissue sections were thus washed with deionized water, incubated for 30 min at room temperature with Perls reagent (5% potassium ferrocyanide and 5% HCl) or Turnbull reagent (5% potassium ferricyanide and 5% HCl), and then washed again with deionized water before incubation at room temperature first for 15 min with 0.05% diaminobenzidine in deionized water and then for 10 min with 0.05% diaminobenzidine in 1% H_2O_2. Sections from control and mutant mice were processed at the same time to allow monitoring and detection of nonspecific staining.

Immunoblot analysis

Total protein extracts were prepared from mouse liver or human HCC specimens by lysis with a solution comprising 50 mM Tris-HCl (pH 7.5), 150 mM NaCl, 0.5% Triton X-100, aprotinin (10 µg/ml), leupeptin (10 µg/ml), 1 mM PMSF, 400 µM Na_3VO_4, 400 µM EDTA, 10 mM NaF, and 10 mM sodium pyrophosphate. The extracts (40 µg of protein) were fractionated by SDS-PAGE on a 10% gel, and the separated proteins were then transferred to a polyvinylidene difluoride membrane (IPVH00010; Millipore). The membrane was exposed to 3% dried skim milk and then incubated overnight at 4°C with primary antibodies to TfR1 (13–6800; Invitrogen), to Hmox1 (sc-10789; Santa Cruz Biotechnology), to Hsp90 (610419; BD Biosciences), to human IRP2 (sc-33682; Santa Cruz Biotechnology), or to mouse IRP2 (generated by K. Iwai, Kyoto University, Kyoto, Japan). Immune complexes were detected with HRP-conjugated secondary antibodies (Promega) and enhanced chemiluminescence reagents (Thermo Fisher Scientific; Nagahama et al., 2001; Foster et al., 2003; Hirano et al., 2013). For analysis of the human HCC specimens, the membrane was also stained with Coomassie Brilliant Blue as a loading control.

RT and real-time PCR analysis

Total RNA was extracted from liver with the use of the Isogen reagent (Nippon Gene). Portions (1 µg) of the purified RNA were then subjected to RT with the use of ReverTra Ace α (Toyobo), and the resulting cDNA was subjected to real-time PCR analysis with SYBR Green PCR Master Mix (Applied Biosystems) and specific primers in a Step One Plus Real-Time PCR System (Applied Biosystems). Data were normalized by the abundance of attachment region–binding protein mRNA. The sequences of the various primers (sense and antisense, respectively) were as follows: 5′-GGACCCGAGAAGACCTCCTT-3′ and 5′-GCACATCAC TCAGAATTTCAATGG-3′ for attachment region–binding protein; 5′-AAGCCGAGAATGCTGAGTTCA-3′ and 5′-GCCGTGTAG ATATGGTACAAGGA-3′ for Hmox1; 5′-AGCGTTCGGTATTAC GATCC-3′ and 5′-AGTACAATCAGGGCTCTTCTCG-3′ for Nqo1; 5′-CATTGAAGTGGTGAAGCACG-3′ and 5′-CTGGACTGTGAG CTGAGTGG-3′ for Gsta1; 5′-CAAACCGATCTCTCGTCGAT-3′ and 5′-AGGAGCAGCAGCTTTTCTTG-3′ for MT2; 5′-TGGGTGGAA CTGCTCGTAAT-3′ and 5′-AGGATGTAGCGTCCAAATGC-3′ for Slc7a11; 5′-GATGGAGCCCATTCCTGAACC-3′ and 5′-CCCTGT ACTTATCCAGGCAGA-3′ for Gpx4; 5′-CCTGAGGGGCTTGAA ATTCAC-3′ and 5′-GTTGGTCTACTTGGAGGAACG-3′ for ACSL4; 5′-GGGAGTCTGGAACATTGTGAA-3′ and 5′-GTGCACATTGTA AGTAGGTGGACT-3′ for PTGS2; 5′-CTGTGGATTTTCGGGTAC GG-3′ and 5′-CCCCTATGGAAGGTGTCTCC-3′ for Chac1; 5′-CCC TCACACTCAGATCATCTTCT-3′ and 5′-GCTACGACGTGGGCT ACAG-3′ for TNFα; 5′-TTAAAAACCTGGATCGGAACCAA-3′ and 5′-GCATTAGCTTCAGATTTACGGGT-3′ for CCL2; and 5′-GCT GCTTTGCCTACCTCTCC-3′ and 5′-TCGAGTGACAAACACGAC TGC-3′ for CCL5.

Biochemical analysis

Serum ALT activity was measured with a standard clinical autoanalyzer.

Statistical analysis

No statistical methods were used to predetermine sample size. Experiments were not randomized. The investigator was blinded to clinical outcome for immunoblot analysis of human HCC specimens. Quantitative data are presented as means ± SD unless indicated otherwise. Comparisons between two groups were performed with the two-tailed Student's *t* test or Mann–Whitney *U* test, and those among three groups were performed by one-way ANOVA followed by a post hoc Tukey test. Differences between survival curves were analyzed with the log-rank nonparametric test. Pearson's correlation analysis was applied to evaluate the relation between protein expression levels (Fig. 8 B). For meta-analysis, a random-effects model (Riley et al., 2011) was adopted within Cochrane Review Manager (RevMan) V.5.3 software to synthesize the result as instructed by the Cochrane community. A P value of <0.05 was considered statistically significant.

Data availability

The RNA-seq data have been deposited in GEO under the accession no. GSE124370. All other relevant data are available from the corresponding authors on reasonable request.

Online supplemental material

Fig. S1 shows that FBXL5 deficiency increases DEN-induced hepatic tumor incidence. Fig. S2 shows that *Alb*-Cre alone does not influence DEN-induced liver carcinogenesis. Fig. S3 shows that a low level of *FBXL5* expression is associated with an increased number of mutations in human HCC. Fig. S4 shows that *FBXL5* expression level is lower in HCC associated with hemochromatosis than in that associated with HBV or HCV infection. Table S1 shows clinical information for the HCC patients and signal intensities of the immunoblot bands in Fig. 8.

Acknowledgments

We thank T. Rouault (National Institutes of Health, Bethesda, MD) for *Irp2*$^{-/-}$ mice; K. Iwai (Kyoto University, Kyoto, Japan) for antibodies to mouse IRP2; E. Koba, K. Tsunematsu, and other laboratory members for technical assistance; A. Ohta for help with preparation of the manuscript; and all patients who donated tissue for this research.

This study was funded in part by KAKENHI grants from the Ministry of Education, Culture, Sports, Science, and Technology of Japan (25221303, 18H05215, and 17H06301).

The authors declare no competing financial interests.

Author contributions: Y. Muto planned and performed experiments with human HCC samples, collected a large portion of mouse experimental data, and wrote the manuscript. T. Moroishi designed the study, performed and analyzed the mouse experiments, and wrote the manuscript. K. Ichihara performed the mouse experiments and RNA-seq. M. Nishiyama provided materials and intellectual support. H. Shimizu and Y. Katayama performed informatics analysis. H. Eguchi, M. Mori, and K. Mimori collected human HCC samples. K. Moriya and K. Koike generated HCVcpTg mice. K.I. Nakayama coordinated the study, oversaw collection and analysis of the results, and wrote the manuscript. All authors discussed the data and commented on the manuscript.

Submitted: 15 May 2018
Revised: 15 January 2019
Accepted: 25 February 2019

References

Asare, G.A., M. Bronz, V. Naidoo, and M.C. Kew. 2007. Interactions between aflatoxin B1 and dietary iron overload in hepatic mutagenesis. *Toxicology*. 234:157–166. https://doi.org/10.1016/j.tox.2007.02.009

Bacon, B.R., P.C. Adams, K.V. Kowdley, L.W. Powell, and A.S. Tavill. American Association for the Study of Liver Diseases. 2011. Diagnosis and management of hemochromatosis: 2011 practice guideline by the American Association for the Study of Liver Diseases. *Hepatology*. 54: 328–343. https://doi.org/10.1002/hep.24330

Britton, L.J., V.N. Subramaniam, and D.H. Crawford. 2016. Iron and non-alcoholic fatty liver disease. *World J. Gastroenterol.* 22:8112–8122. https://doi.org/10.3748/wjg.v22.i36.8112

Budczies, J., F. Klauschen, B.V. Sinn, B. Győrffy, W.D. Schmitt, S. Darb-Esfahani, and C. Denkert. 2012. Cutoff Finder: a comprehensive and straightforward Web application enabling rapid biomarker cutoff optimization. *PLoS One*. 7:e51862. https://doi.org/10.1371/journal.pone.0051862

Cerami, E., J. Gao, U. Dogrusoz, B.E. Gross, S.O. Sumer, B.A. Aksoy, A. Jacobsen, C.J. Byrne, M.L. Heuer, E. Larsson, et al. 2012. The cBio cancer genomics portal: an open platform for exploring multidimensional cancer genomics data. *Cancer Discov.* 2:401–404. https://doi.org/10.1158/2159-8290.CD-12-0095

Chapoutot, C., M. Esslimani, Z. Joomaye, J. Ramos, P. Perney, C. Laurent, P. Fabbro-Peray, D. Larrey, J. Domergue, and F. Blanc. 2000. Liver iron excess in patients with hepatocellular carcinoma developed on viral C cirrhosis. *Gut*. 46:711–714. https://doi.org/10.1136/gut.46.5.711

Chen, M.S., S.F. Wang, C.Y. Hsu, P.H. Yin, T.S. Yeh, H.C. Lee, and L.M. Tseng. 2017. CHAC1 degradation of glutathione enhances cystine-starvation-induced necroptosis and ferroptosis in human triple negative breast cancer cells via the GCN2-eIF2α-ATF4 pathway. *Oncotarget*. 8: 114588–114602. https://doi.org/10.18632/oncotarget.23055

Chen, Z.W., B. Liu, N.W. Tang, Y.H. Xu, X.Y. Ye, Z.M. Li, X.M. Niu, S.P. Shen, S. Lu, and L. Xu. 2014. FBXL5-mediated degradation of single-stranded DNA-binding protein hSSB1 controls DNA damage response. *Nucleic Acids Res.* 42:11560–11569. https://doi.org/10.1093/nar/gku876

Cheung, K.F., J. Zhao, Y. Hao, X. Li, A.W. Lowe, A.S. Cheng, J.J. Sung, and J. Yu. 2013. CITED2 is a novel direct effector of peroxisome proliferator-activated receptor γ in suppressing hepatocellular carcinoma cell growth. *Cancer*. 119:1217–1226. https://doi.org/10.1002/cncr.27865

Cibulskis, K., M.S. Lawrence, S.L. Carter, A. Sivachenko, D. Jaffe, C. Sougnez, S. Gabriel, M. Meyerson, E.S. Lander, and G. Getz. 2013. Sensitive detection of somatic point mutations in impure and heterogeneous cancer samples. *Nat. Biotechnol.* 31:213–219. https://doi.org/10.1038/nbt.2514

Cichoż-Lach, H., and A. Michalak. 2014. Oxidative stress as a crucial factor in liver diseases. *World J. Gastroenterol.* 20:8082–8091. https://doi.org/10.3748/wjg.v20.i25.8082

Cooperman, S.S., E.G. Meyron-Holtz, H. Olivierre-Wilson, M.C. Ghosh, J.P. McConnell, and T.A. Rouault. 2005. Microcytic anemia, erythropoietic protoporphyria, and neurodegeneration in mice with targeted deletion of iron-regulatory protein 2. *Blood*. 106:1084–1091. https://doi.org/10.1182/blood-2004-12-4703

Coudray, A., A.M. Battenhouse, P. Bucher, and V.R. Iyer. 2018. Detection and benchmarking of somatic mutations in cancer genomes using RNA-seq data. *PeerJ*. 6:e5362. https://doi.org/10.7717/peerj.5362

Dang, H., W. Ding, D. Emerson, and C.B. Rountree. 2011. Snail1 induces epithelial-to-mesenchymal transition and tumor initiating stem cell characteristics. *BMC Cancer*. 11:396. https://doi.org/10.1186/1471-2407-11-396

Deugnier, Y.M., P. Charalambous, D. Le Quilleuc, B. Turlin, J. Searle, P. Brissot, L.W. Powell, and J.W. Halliday. 1993. Preneoplastic significance of hepatic iron-free foci in genetic hemochromatosis: a study of 185 patients. *Hepatology*. 18:1363–1369.

Dixon, S.J., K.M. Lemberg, M.R. Lamprecht, R. Skouta, E.M. Zaitsev, C.E. Gleason, D.N. Patel, A.J. Bauer, A.M. Cantley, W.S. Yang, et al. 2012.

Ferroptosis: an iron-dependent form of nonapoptotic cell death. *Cell.* 149:1060–1072. https://doi.org/10.1016/j.cell.2012.03.042

Dobin, A., and T.R. Gingeras. 2015. Mapping RNA-seq Reads with STAR. *Curr. Protoc. Bioinformatics.* 51:1–19. https://doi.org/10.1002/0471250953.bi1114s51

Doll, S., B. Proneth, Y.Y. Tyurina, E. Panzilius, S. Kobayashi, I. Ingold, M. Irmler, J. Beckers, M. Aichler, A. Walch, et al. 2017. ACSL4 dictates ferroptosis sensitivity by shaping cellular lipid composition. *Nat. Chem. Biol.* 13:91–98. https://doi.org/10.1038/nchembio.2239

El-Serag, H.B. 2011. Hepatocellular carcinoma. *N. Engl. J. Med.* 365:1118–1127. https://doi.org/10.1056/NEJMra1001683

Farazi, P.A., and R.A. DePinho. 2006. Hepatocellular carcinoma pathogenesis: from genes to environment. *Nat. Rev. Cancer.* 6:674–687. https://doi.org/10.1038/nrc1934

Felton, C., E.D. Lustbader, C. Merten, and B.S. Blumberg. 1979. Serum iron levels and response to hepatitis B virus. *Proc. Natl. Acad. Sci. USA.* 76:2438–2441. https://doi.org/10.1073/pnas.76.5.2438

Foster, J.S., R.I. Fernando, N. Ishida, K.I. Nakayama, and J. Wimalasena. 2003. Estrogens down-regulate p27Kip1 in breast cancer cells through Skp2 and through nuclear export mediated by the ERK pathway. *J. Biol. Chem.* 278:41355–41366. https://doi.org/10.1074/jbc.M302830200

Fujita, N., R. Sugimoto, M. Takeo, N. Urawa, R. Mifuji, H. Tanaka, Y. Kobayashi, M. Iwasa, S. Watanabe, Y. Adachi, and M. Kaito. 2007. Hepcidin expression in the liver: relatively low level in patients with chronic hepatitis C. *Mol. Med.* 13:97–104. https://doi.org/10.2119/2006-00057.Fujita

Galy, B., D. Ferring, B. Minana, O. Bell, H.G. Janser, M. Muckenthaler, K. Schümann, and M.W. Hentze. 2005. Altered body iron distribution and microcytosis in mice deficient in iron regulatory protein 2 (IRP2). *Blood.* 106:2580–2589. https://doi.org/10.1182/blood-2005-04-1365

Ganne-Carrié, N., C. Christidis, C. Chastang, M. Ziol, F. Chapel, F. Imbert-Bismut, J.C. Trinchet, C. Guettier, and M. Beaugrand. 2000. Liver iron is predictive of death in alcoholic cirrhosis: a multivariate study of 229 consecutive patients with alcoholic and/or hepatitis C virus cirrhosis: a prospective follow up study. *Gut.* 46:277–282. https://doi.org/10.1136/gut.46.2.277

Gao, J., B.A. Aksoy, U. Dogrusoz, G. Dresdner, B. Gross, S.O. Sumer, Y. Sun, A. Jacobsen, R. Sinha, E. Larsson, et al. 2013. Integrative analysis of complex cancer genomics and clinical profiles using the cBioPortal. *Sci. Signal.* 6:pl1. https://doi.org/10.1126/scisignal.2004088

Girelli, D., M. Pasino, J.B. Goodnough, E. Nemeth, M. Guido, A. Castagna, F. Busti, N. Campostrini, N. Martinelli, I. Vantini, et al. 2009. Reduced serum hepcidin levels in patients with chronic hepatitis C. *J. Hepatol.* 51:845–852. https://doi.org/10.1016/j.jhep.2009.06.027

Grafodatskaya, D., B.H. Chung, D.T. Butcher, A.L. Turinsky, S.J. Goodman, S. Choufani, Y.A. Chen, Y. Lou, C. Zhao, R. Rajendram, et al. 2013. Multilocus loss of DNA methylation in individuals with mutations in the histone H3 lysine 4 demethylase KDM5C. *BMC Med. Genomics.* 6:1. https://doi.org/10.1186/1755-8794-6-1

Guichard, C., G. Amaddeo, S. Imbeaud, Y. Ladeiro, L. Pelletier, I.B. Maad, J. Calderaro, P. Bioulac-Sage, M. Letexier, F. Degos, et al. 2012. Integrated analysis of somatic mutations and focal copy-number changes identifies key genes and pathways in hepatocellular carcinoma. *Nat. Genet.* 44:694–698. https://doi.org/10.1038/ng.2256

Hentze, M.W., M.U. Muckenthaler, B. Galy, and C. Camaschella. 2010. Two to tango: regulation of Mammalian iron metabolism. *Cell.* 142:24–38. https://doi.org/10.1016/j.cell.2010.06.028

Hirano, A., K. Yumimoto, R. Tsunematsu, M. Matsumoto, M. Oyama, H. Kozuka-Hata, T. Nakagawa, D. Lanjakornsiripan, K.I. Nakayama, and Y. Fukada. 2013. FBXL21 regulates oscillation of the circadian clock through ubiquitination and stabilization of cryptochromes. *Cell.* 152:1106–1118. https://doi.org/10.1016/j.cell.2013.01.054

Hirata, H., K. Sugimachi, H. Komatsu, M. Ueda, T. Masuda, R. Uchi, S. Sakimura, S. Nambara, T. Saito, Y. Shinden, et al. 2016. Decreased Expression of Fructose-1,6-bisphosphatase Associates with Glucose Metabolism and Tumor Progression in Hepatocellular Carcinoma. *Cancer Res.* 76:3265–3276. https://doi.org/10.1158/0008-5472.CAN-15-2601

Ji, X., S. Jin, X. Qu, K. Li, H. Wang, H. He, F. Guo, and L. Dong. 2015. Lysine-specific demethylase 5C promotes hepatocellular carcinoma cell invasion through inhibition BMP7 expression. *BMC Cancer.* 15:801. https://doi.org/10.1186/s12885-015-1798-4

Jiang, L., N. Kon, T. Li, S.J. Wang, T. Su, H. Hibshoosh, R. Baer, and W. Gu. 2015. Ferroptosis as a p53-mediated activity during tumour suppression. *Nature.* 520:57–62. https://doi.org/10.1038/nature14344

Kamata, H., S. Honda, S. Maeda, L. Chang, H. Hirata, and M. Karin. 2005. Reactive oxygen species promote TNFalpha-induced death and sustained JNK activation by inhibiting MAP kinase phosphatases. *Cell.* 120:649–661. https://doi.org/10.1016/j.cell.2004.12.041

Katayama, Y., M. Nishiyama, H. Shoji, Y. Ohkawa, A. Kawamura, T. Sato, M. Suyama, T. Takumi, T. Miyakawa, and K.I. Nakayama. 2016. CHD8 haploinsufficiency results in autistic-like phenotypes in mice. *Nature.* 537:675–679. https://doi.org/10.1038/nature19357

Kato, J., K. Miyanishi, M. Kobune, T. Nakamura, K. Takada, R. Takimoto, Y. Kawano, S. Takahashi, M. Takahashi, Y. Sato, et al. 2007. Long-term phlebotomy with low-iron diet therapy lowers risk of development of hepatocellular carcinoma from chronic hepatitis C. *J. Gastroenterol.* 42:830–836. https://doi.org/10.1007/s00535-007-2095-z

Knight, B., G.C. Yeoh, K.L. Husk, T. Ly, L.J. Abraham, C. Yu, J.A. Rhim, and N. Fausto. 2000. Impaired preneoplastic changes and liver tumor formation in tumor necrosis factor receptor type 1 knockout mice. *J. Exp. Med.* 192:1809–1818. https://doi.org/10.1084/jem.192.12.1809

LaVaute, T., S. Smith, S. Cooperman, K. Iwai, W. Land, E. Meyron-Holtz, S.K. Drake, G. Miller, M. Abu-Asab, M. Tsokos, et al. 2001. Targeted deletion of the gene encoding iron regulatory protein-2 causes misregulation of iron metabolism and neurodegenerative disease in mice. *Nat. Genet.* 27:209–214. https://doi.org/10.1038/84859

Li, B., X. Wang, N. Rasheed, Y. Hu, S. Boast, T. Ishii, K. Nakayama, K.I. Nakayama, and S.P. Goff. 2004. Distinct roles of c-Abl and Atm in oxidative stress response are mediated by protein kinase C delta. *Genes Dev.* 18:1824–1837. https://doi.org/10.1101/gad.1223504

Li, X., W. Yao, Y. Yuan, P. Chen, B. Li, J. Li, R. Chu, H. Song, D. Xie, X. Jiang, and H. Wang. 2017. Targeting of tumour-infiltrating macrophages via CCL2/CCR2 signalling as a therapeutic strategy against hepatocellular carcinoma. *Gut.* 66:157–167. https://doi.org/10.1136/gutjnl-2015-310514

Luedde, T., N. Kaplowitz, and R.F. Schwabe. 2014. Cell death and cell death responses in liver disease: mechanisms and clinical relevance. *Gastroenterology.* 147:765–783.e4. https://doi.org/10.1053/j.gastro.2014.07.018

Machado-Oliveira, G., E. Guerreiro, A.C. Matias, J. Facucho-Oliveira, I. Pacheco-Leyva, and J. Bragança. 2015. FBXL5 modulates HIF-1α transcriptional activity by degradation of CITED2. *Arch. Biochem. Biophys.* 576:61–72. https://doi.org/10.1016/j.abb.2015.04.012

Maeda, S., H. Kamata, J.L. Luo, H. Leffert, and M. Karin. 2005. IKKbeta couples hepatocyte death to cytokine-driven compensatory proliferation that promotes chemical hepatocarcinogenesis. *Cell.* 121:977–990. https://doi.org/10.1016/j.cell.2005.04.014

Mao, W., Y. Hu, Y. Lou, Y. Chen, and J. Zhang. 2015. Abnormal serum iron markers in chronic hepatitis B virus infection may be because of liver injury. *Eur. J. Gastroenterol. Hepatol.* 27:130–136. https://doi.org/10.1097/MEG.0000000000000247

Marquardt, J.U., J.B. Andersen, and S.S. Thorgeirsson. 2015. Functional and genetic deconstruction of the cellular origin in liver cancer. *Nat. Rev. Cancer.* 15:653–667. https://doi.org/10.1038/nrc4017

Martinelli, A.L., A.B. Filho, R.F. Franco, M.H. Tavella, L.N. Ramalho, S. Zucoloto, S.S. Rodrigues, and M.A. Zago. 2004. Liver iron deposits in hepatitis B patients: association with severity of liver disease but not with hemochromatosis gene mutations. *J. Gastroenterol. Hepatol.* 19:1036–1041. https://doi.org/10.1111/j.1440-1746.2004.03410.x

McKenna, A., M. Hanna, E. Banks, A. Sivachenko, K. Cibulskis, A. Kernytsky, K. Garimella, D. Altshuler, S. Gabriel, M. Daly, and M.A. DePristo. 2010. The Genome Analysis Toolkit: a MapReduce framework for analyzing next-generation DNA sequencing data. *Genome Res.* 20:1297–1303. https://doi.org/10.1101/gr.107524.110

Mohs, A., N. Kuttkat, J. Reißing, H.W. Zimmermann, R. Sonntag, A. Proudfoot, S.A. Youssef, A. de Bruin, F.J. Cubero, and C. Trautwein. 2017. Functional role of CCL5/RANTES for HCC progression during chronic liver disease. *J. Hepatol.* 66:743–753. https://doi.org/10.1016/j.jhep.2016.12.011

Moriya, K., H. Fujie, Y. Shintani, H. Yotsuyanagi, T. Tsutsumi, K. Ishibashi, Y. Matsuura, S. Kimura, T. Miyamura, and K. Koike. 1998. The core protein of hepatitis C virus induces hepatocellular carcinoma in transgenic mice. *Nat. Med.* 4:1065–1067. https://doi.org/10.1038/2053

Moroishi, T., M. Nishiyama, Y. Takeda, K. Iwai, and K.I. Nakayama. 2011. The FBXL5-IRP2 axis is integral to control of iron metabolism in vivo. *Cell Metab.* 14:339–351. https://doi.org/10.1016/j.cmet.2011.07.011

Muto, Y., M. Nishiyama, A. Nita, T. Moroishi, and K.I. Nakayama. 2017. Essential role of FBXL5-mediated cellular iron homeostasis in maintenance of hematopoietic stem cells. *Nat. Commun.* 8:16114. https://doi.org/10.1038/ncomms16114

Nagahama, H., S. Hatakeyama, K. Nakayama, M. Nagata, K. Tomita, and K. Nakayama. 2001. Spatial and temporal expression patterns of the cyclin-dependent kinase (CDK) inhibitors p27Kip1 and p57Kip2 during mouse development. *Anat. Embryol. (Berl.)*. 203:77–87. https://doi.org/10.1007/s004290000146

Nahon, P., A. Sutton, P. Rufat, M. Ziol, G. Thabut, P.O. Schischmanoff, D. Vidaud, N. Charnaux, P. Couvert, N. Ganne-Carrie, et al. 2008. Liver iron, HFE gene mutations, and hepatocellular carcinoma occurrence in patients with cirrhosis. *Gastroenterology*. 134:102–110. https://doi.org/10.1053/j.gastro.2007.10.038

Nanba, S., F. Ikeda, N. Baba, K. Takaguchi, T. Senoh, T. Nagano, H. Seki, Y. Takeuchi, Y. Moritou, T. Yasunaka, et al. 2016. Association of hepatic oxidative stress and iron dysregulation with HCC development after interferon therapy in chronic hepatitis C. *J. Clin. Pathol.* 69:226–233. https://doi.org/10.1136/jclinpath-2015-203215

Naugler, W.E., T. Sakurai, S. Kim, S. Maeda, K. Kim, A.M. Elsharkawy, and M. Karin. 2007. Gender disparity in liver cancer due to sex differences in MyD88-dependent IL-6 production. *Science*. 317:121–124. https://doi.org/10.1126/science.1140485

Neums, L., S. Suenaga, P. Beyerlein, S. Anders, D. Koestler, A. Mariani, and J. Chien. 2018. VaDiR: an integrated approach to Variant Detection in RNA. *Gigascience*. 7. https://doi.org/10.1093/gigascience/gix122

Ngo, H.K.C., D.H. Kim, Y.N. Cha, H.K. Na, and Y.J. Surh. 2017. Nrf2 Mutagenic Activation Drives Hepatocarcinogenesis. *Cancer Res.* 77:4797–4808.

Niederau, C., R. Fischer, A. Pürschel, W. Stremmel, D. Häussinger, and G. Strohmeyer. 1996. Long-term survival in patients with hereditary hemochromatosis. *Gastroenterology*. 110:1107–1119. https://doi.org/10.1053/gast.1996.v110.pm8613000

Nilsson, L., P. Edén, E. Olsson, R. Månsson, I. Astrand-Grundström, B. Strömbeck, K. Theilgaard-Mönch, K. Anderson, R. Hast, E. Hellström-Lindberg, et al. 2007. The molecular signature of MDS stem cells supports a stem-cell origin of 5q myelodysplastic syndromes. *Blood*. 110:3005–3014. https://doi.org/10.1182/blood-2007-03-079368

Postic, C., and M.A. Magnuson. 2000. DNA excision in liver by an albumin-Cre transgene occurs progressively with age. *Genesis*. 26:149–150. https://doi.org/10.1002/(SICI)1526-968X(200002)26:2<149::AID-GENE16>3.0.CO;2-V

Riley, R.D., J.P. Higgins, and J.J. Deeks. 2011. Interpretation of random effects meta-analyses. *BMJ*. 342(feb10 2):d549. https://doi.org/10.1136/bmj.d549

Roessler, S., H.L. Jia, A. Budhu, M. Forgues, Q.H. Ye, J.S. Lee, S.S. Thorgeirsson, Z. Sun, Z.Y. Tang, L.X. Qin, and X.W. Wang. 2010. A unique metastasis gene signature enables prediction of tumor relapse in early-stage hepatocellular carcinoma patients. *Cancer Res.* 70:10202–10212. https://doi.org/10.1158/0008-5472.CAN-10-2607

Ruiz, J.C., S.D. Walker, S.A. Anderson, R.S. Eisenstein, and R.K. Bruick. 2013. F-box and leucine-rich repeat protein 5 (FBXL5) is required for maintenance of cellular and systemic iron homeostasis. *J. Biol. Chem.* 288:552–560. https://doi.org/10.1074/jbc.M112.426171

Salahudeen, A.A., J.W. Thompson, J.C. Ruiz, H.W. Ma, L.N. Kinch, Q. Li, N.V. Grishin, and R.K. Bruick. 2009. An E3 ligase possessing an iron-responsive hemerythrin domain is a regulator of iron homeostasis. *Science*. 326:722–726. https://doi.org/10.1126/science.1176326

Sarma, D.S., P.M. Rao, and S. Rajalakshmi. 1986. Liver tumour promotion by chemicals: models and mechanisms. *Cancer Surv.* 5:781–798.

Senba, M., T. Nakamura, and H. Itakura. 1985. Statistical analysis of relationship between iron accumulation and hepatitis B surface antigen. *Am. J. Clin. Pathol.* 84:340–342. https://doi.org/10.1093/ajcp/84.3.340

Sorrentino, P., S. D'Angelo, U. Ferbo, P. Micheli, A. Bracigliano, and R. Vecchione. 2009. Liver iron excess in patients with hepatocellular carcinoma developed on non-alcoholic steato-hepatitis. *J. Hepatol.* 50:351–357. https://doi.org/10.1016/j.jhep.2008.09.011

Terada, T., and Y. Nakanuma. 1989. Iron-negative foci in siderotic macroregenerative nodules in human cirrhotic liver. A marker of incipient neoplastic lesions. *Arch. Pathol. Lab. Med.* 113:916–920.

Tseng, H.H., J.G. Chang, Y.H. Hwang, K.T. Yeh, Y.L. Chen, and H.S. Yu. 2009. Expression of hepcidin and other iron-regulatory genes in human hepatocellular carcinoma and its clinical implications. *J. Cancer Res. Clin. Oncol.* 135:1413–1420. https://doi.org/10.1007/s00432-009-0585-5

Valenti, L., A.L. Fracanzani, E. Bugianesi, P. Dongiovanni, E. Galmozzi, E. Vanni, E. Canavesi, E. Lattuada, G. Roviaro, G. Marchesini, and S. Fargion. 2010. HFE genotype, parenchymal iron accumulation, and liver fibrosis in patients with nonalcoholic fatty liver disease. *Gastroenterology*. 138:905–912. https://doi.org/10.1053/j.gastro.2009.11.013

Vashisht, A.A., K.B. Zumbrennen, X. Huang, D.N. Powers, A. Durazo, D. Sun, N. Bhaskaran, A. Persson, M. Uhlen, O. Sangfelt, et al. 2009. Control of iron homeostasis by an iron-regulated ubiquitin ligase. *Science*. 326:718–721. https://doi.org/10.1126/science.1176333

Viñas-Castells, R., Á. Frías, E. Robles-Lanuza, K. Zhang, G.D. Longmore, A. García de Herreros, and V.M. Díaz. 2014. Nuclear ubiquitination by FBXL5 modulates Snail1 DNA binding and stability. *Nucleic Acids Res.* 42:1079–1094. https://doi.org/10.1093/nar/gkt935

Wang, H., P. An, E. Xie, Q. Wu, X. Fang, H. Gao, Z. Zhang, Y. Li, X. Wang, J. Zhang, et al. 2017. Characterization of ferroptosis in murine models of hemochromatosis. *Hepatology*. 66:449–465. https://doi.org/10.1002/hep.29117

Wu, W., H. Ding, J. Cao, and W. Zhang. 2015. FBXL5 inhibits metastasis of gastric cancer through suppressing Snail1. *Cell. Physiol. Biochem.* 35:1764–1772. https://doi.org/10.1159/000373988

Yang, W.S., R. SriRamaratnam, M.E. Welsch, K. Shimada, R. Skouta, V.S. Viswanathan, J.H. Cheah, P.A. Clemons, A.F. Shamji, C.B. Clish, et al. 2014. Regulation of ferroptotic cancer cell death by GPX4. *Cell*. 156:317–331. https://doi.org/10.1016/j.cell.2013.12.010

Yokobori, T., K. Mimori, M. Iwatsuki, H. Ishii, I. Onoyama, T. Fukagawa, H. Kuwano, K.I. Nakayama, and M. Mori. 2009. p53-Altered FBXW7 expression determines poor prognosis in gastric cancer cases. *Cancer Res.* 69:3788–3794. https://doi.org/10.1158/0008-5472.CAN-08-2846

Zavattari, P., A. Perra, S. Menegon, M.A. Kowalik, A. Petrelli, M.M. Angioni, A. Follenzi, L. Quagliata, G.M. Ledda-Columbano, L. Terracciano, et al. 2015. Nrf2, but not β-catenin, mutation represents an early event in rat hepatocarcinogenesis. *Hepatology*. 62:851–862. https://doi.org/10.1002/hep.27790

Zhang, M., C. Zhang, L. Zhang, Q. Yang, S. Zhou, Q. Wen, and J. Wang. 2015. Nrf2 is a potential prognostic marker and promotes proliferation and invasion in human hepatocellular carcinoma. *BMC Cancer*. 15:531. https://doi.org/10.1186/s12885-015-1541-1

Zhang, N., J. Liu, X. Ding, F. Aikhionbare, C. Jin, and X. Yao. 2007. FBXL5 interacts with p150Glued and regulates its ubiquitination. *Biochem. Biophys. Res. Commun.* 359:34–39. https://doi.org/10.1016/j.bbrc.2007.05.068